applied sciences

MDPI

Article

Assessment of Vegetation Cover and Rainfall Infiltration Effects on Slope Stability

Gaoliang Tao [1,2,3], Lingsan Guo [1,2], Henglin Xiao [4,*], Qingsheng Chen [1,2], Sanjay Nimbalkar [5], Shiju Feng [1,2] and Zhijia Wu [1,2]

[1] Key Laboratory of Intelligent Health Perception and Ecological Restoration of Rivers and Lakes, Ministry of Education, Hubei University of Technology, Wuhan 430068, China; tgl1979@126.com (G.T.); gls19990622@126.com (L.G.); chqsh2006@163.com (Q.C.); fsj20231016@163.com (S.F.); wzj2301214319@163.com (Z.W.)
[2] Hubei Key Laboratory of Environmental Geotechnology and Ecological Remediation for Lake & River, Innovation Demonstration Base of Ecological Environment, Geotechnical and Ecological Restoration of Rivers and Lakes, Hubei University of Technology, Wuhan 430068, China
[3] School of Intelligent Construction, Wuchang University of Technology, No.16, Jiangxia Avenue, Jiangxia District, Wuhan 430223, China
[4] State Key Laboratory of Precision Blasting, Jianghan University, Wuhan 430056, China
[5] School of Civil and Environmental Engineering, University of Technology Sydney, 15 Broadway, Ultimo, NSW 2007, Australia; sanjay.nimbalkar@uts.edu.au
* Correspondence: xiao-henglin@163.com

Abstract

Investigating rainfall infiltration mechanisms and slope stability dynamics under varying vegetation cover conditions is essential for advancing ecological slope protection methodologies. This research focuses on large-scale outdoor slope models, with the objective of monitoring soil moisture variations in real-time during rainfall events on four types of slopes: bare, herbaceous, shrub, and mixed herb–shrub planting. Combining direct shear tests for unsaturated soil with numerical simulations, and considering the weakening effect of water on shear strength, this study analyzes slope stability. The findings reveal significant spatial variations in rainfall infiltration rates, with maximum values recorded at a burial depth of 0.2 m, declining as the burial depth increases. Different types of vegetation have distinct impacts on slope infiltration patterns: herbaceous increases cumulative infiltration by 21.32%, while shrub reduces it by 61.06%. The numerically simulated moisture content values demonstrate strong congruence with field-measured data. Compared with monoculture herbaceous or shrub root systems, the mixed herb–shrub root system exhibits the most significant enhancement effects on shear strength parameters. Under high water content conditions, root systems demonstrate substantially greater improvement in cohesion than in internal friction angle. Before rainfall, shrub vegetation contributed the most significant improvement to the safety factor, increasing it from 2.766 to 3.046, followed by herbaceous and mixed herb–shrub vegetation, which raised it to 2.81 and 2.948. After rainfall, mixed herb–shrub vegetation demonstrated the greatest enhancement of the safety factor, elevating it from 1.139 to 1.361, followed by herbaceous and shrub vegetation, which increased it to 1.192 and 1.275. The study offers preliminary insights and a scientific basis for the specific conditions tested for selecting and optimizing eco-friendly slope protection measures.

Keywords: vegetated slope; rainfall infiltration; slope stability; shear strength; slip plane

Academic Editor: Fernando Rocha

Received: 2 August 2025
Revised: 2 September 2025
Accepted: 3 September 2025
Published: 8 September 2025

Citation: Tao, G.; Guo, L.; Xiao, H.; Chen, Q.; Nimbalkar, S.; Feng, S.; Wu, Z. Assessment of Vegetation Cover and Rainfall Infiltration Effects on Slope Stability. *Appl. Sci.* **2025**, *15*, 9831. https://doi.org/10.3390/app15179831

1. Introduction

Landslides are frequently observed in many regions, with over 90% of them induced by natural rainfall [1–3]. Vegetation-based slope protection is an effective ecological slope stabilization method that utilizes the hydrological and mechanical effects of plant roots to regulate soil properties and enhance slope stability [4–8].

Extensive research efforts have led to measurable advancements in this field. In hydrologic effects, the plant canopy and litter layer can intercept rainfall and reduce surface erosion [9], while root systems significantly alter the hydraulic properties of soil, thereby regulating rainfall infiltration patterns and pore water pressure distribution within slopes. For instance, a comprehensive review by Löbmann et al. [10] emphasizes that herbaceous vegetation plays a critical and complex role in slope stability, primarily through root reinforcement, though its effects on hydrological processes may be species-specific and context-dependent [11,12]. Wu et al. [13] and Nguyen et al. [14] employed limit equilibrium methods, indicating that rainfall characteristics are primary external triggers for instability. Qi and Hu [15] found that vegetated slope protection utilizes vegetation's mechanisms of moisture retention and soil conservation to stabilize slope and protect surfaces.

In mechanical effects, the mechanical reinforcement provided by plant roots is a key factor in enhancing the shear strength of soil. This reinforcement is typically achieved through additional root cohesion. Studies have shown that different types of vegetation provide varying degrees of stabilization. For example, herbaceous plants, with their dense and fibrous root systems, are highly effective in stabilizing surface soils [16,17], while shrubs, with their deeper and stronger taproot systems, provide anchoring effects that stabilize deeper slope layers [12,18,19]. Yu et al. [20] used the self-built experimental area around the Xining Basin as an example to evaluate the reinforcement effect of plant roots on slope soil. Yildiz et al. [21] explored the extent to which vegetation enhances slope stability, emphasizing the quantification of vegetation's contribution to soil shear strength as a critical determinant of slope safety factors. Yi et al. [22] posited that vegetation plays a crucial role in stabilizing soil on slope and preventing soil erosion. Cheng et al. [23] comprehensively evaluated the hydraulic and mechanical properties of plant–soil through on site tests combined with indoor triaxial tests, the results showed that vetiver reinforced soil more effectively than herbaceous.

Numerical simulation has been widely employed to investigate these effects. For instance. Ji and Yang [24] conducted finite element analyses of vegetated slopes with different root configurations using PLAXIS 3D AE software. Kokutse et al. [25] applied the strength reduction method to evaluate the stability of herbaceous and shrub vegetation on various slope types. Their findings underscore the significant role of rainfall among influencing factors, highlighting its importance in slope stability analysis.

However, current research has predominantly focused on the individual effects of herbaceous [16,17] or shrub vegetation [12,18,19]. For instance, studies by Marzini et al. and Löbmann et al. have provided valuable insights into the reinforcement effects of single-species vegetation [10,12], yet they primarily examined them in isolation. There remains a relative scarcity of studies that directly compare the synergistic or antagonistic interactions within mixed vegetation systems under identical conditions. Furthermore, the coupling mechanisms among vegetation type, associated hydrological changes (infiltration/runoff), and the mechanical response of slope systems require more comprehensive investigation. While some studies have explored hydrological or mechanical effects separately, an integrated analysis that captures their complex interplay in mixed planting schemes is still lacking [26–28].

Consequently, it is imperative to explore the rainfall infiltration and stability of slopes with single-species and mixed-species vegetation planting under rainfall condition. This

study carries out extensive slope model rainfall experiments to explore the impact of various vegetation planting modes on slope infiltration patterns, specifically focusing on bare, herbaceous, shrub, and mixed herb–shrub slope. Through the combination of laboratory experiments and numerical simulations, a numerical model of slopes is developed, considering the influence of soil moisture content on shear strength parameters and the mechanical effects of root systems. This study further explores the impact mechanism of different vegetation planting forms on slope stability under rainfall.

2. Rainfall Infiltration Testing in Large-Scale Vegetated Slopes

2.1. Study Area

This study was conducted at the Ecological Restoration Pilot Base of Hubei University of Technology, located in Wuhan, Hubei Province, China. The city experiences a humid subtropical monsoon climate, characterized by distinct seasonal variations with hot, humid summers and cool, damp winters. The mean annual temperature is 16.7 °C, and the average annual rainfall is approximately 1260 mm, the majority of which occurs during the intense monsoon season between June and August. Geotechnically, the site is situated on typical Quaternary alluvial deposits of the Yangtze River Plain, which are highly representative of the region's geomorphic conditions. This site was selected not only due to its climatic and geological representativeness but also because it offers comprehensive experimental facilities, including advanced monitoring instrumentation and controlled slope models, which are essential for large-scale, long-term hydrological and geotechnical monitoring [29].

2.2. Soil Basic Parameters

The test soil was obtained from a construction foundation pit in the Nanhu, Hongshan District, Wuhan, with a sampling depth of approximately 5 to 7 m. According to the GB/T 50123-2019 [30] standard for geotechnical testing methods, the basic physical indicators of the soil sample are measured, as shown in Table 1. According to the USDA soil classification system in the United States, the content of sand particles (>0.05 mm), silt particles (0.05–0.002 mm), and clay particles (<0.002 mm) in the experimental soil is 13%, 61%, and 26%, respectively. The soil sample is classified as loam, $C_u = d_{60}/d_{10} = 23.77 > 5$, $C_c = d_{30}^2/(d_{60} \times d_{10}) = 1.83$, Between 1~3, indicating a well-graded particle size distribution, as shown in Figure 1.

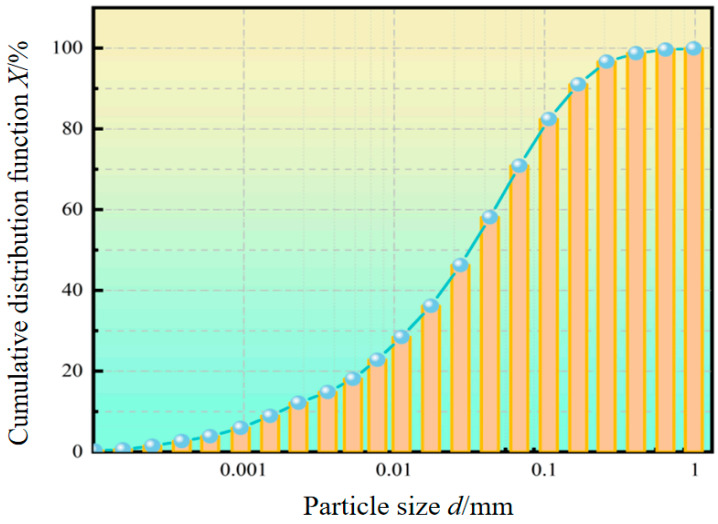

Figure 1. Particle size distribution curve of the soil.

Table 1. Basic physical properties of Wuhan loam.

Name	Liquid Limit ω_L	Plastic Limit ω_P	Maximum Dry Density ρ_d	Optimum Moisture Content ω_{op}	Natural Moisture Content ω
Loam	41%	23%	1.75 g/cm^3	20%	15.6%

2.3. Model Design

The experimental site is located at the ecological restoration pilot base of Hubei University of Technology in Wuhan. To simulate a realistic yet controlled slope environment, the slope model was constructed with concrete aerated bricks and coated with cement mortar for structural stability and surface integrity. The crest and sides were lined with waterproof materials to prevent rainwater infiltration and mutual interference between models. Furthermore, to facilitate prompt rainwater drainage, a 30 cm wide and 20 cm deep collection trough was situated at the foot of the slope.

The soil moisture monitoring equipment employs RS485-type soil moisture transmitter produced by Shandong Jianda Renke Company, primarily consisting of sensor and data acquisition, which are connected in parallel, the relevant technical parameters are shown in Table 2. To meet the demand for long-term accurate detection of changes in slope moisture content, the sensors were calibrated for pressure, temperature, and sensitivity before the experiment. After precise calibration, the sensors were buried along the slope's axis at depths of 0.2 m, 0.4 m, 0.6 m, and 1.0 m to capture the moisture profile. During the backfilling process, to minimize disturbance and maintain natural soil stratification, the soil was layered in accordance with the sensor distribution, with compaction applied along the parallel slope direction for each soil layer. The weather station employs a pH automatic weather station produced by Wuhan Xinpu Technology Company to monitor meteorological conditions at the test site in real time, as shown in Figure 2. The real scene of the model and the sensor layout are shown in Figures 3 and 4.

Table 2. Technical parameters of sensors.

Parameter	Range	Accuracy, A	Resolution, R	Response Time, t	Measurement Area, A_m
Water content, θ(%)	0~100%	±2.5%	0.1%	<1 s	Φ7 × 7 cm cylinder

(**a**) (**b**) (**c**)

Figure 2. Equipment tested; (**a**) moisture sensor; (**b**) data acquisition; (**c**) pH automatic weather station.

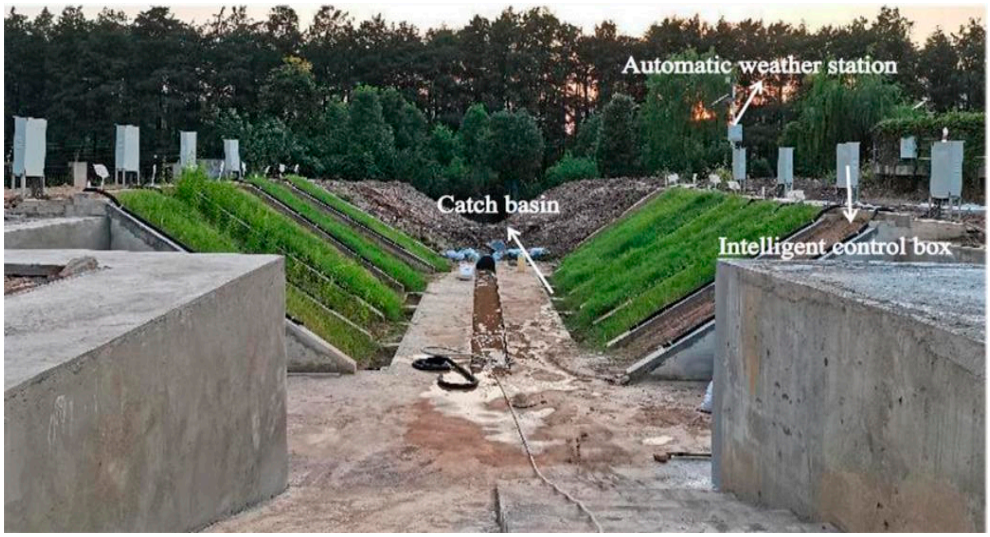

Figure 3. Field photograph of the slope model.

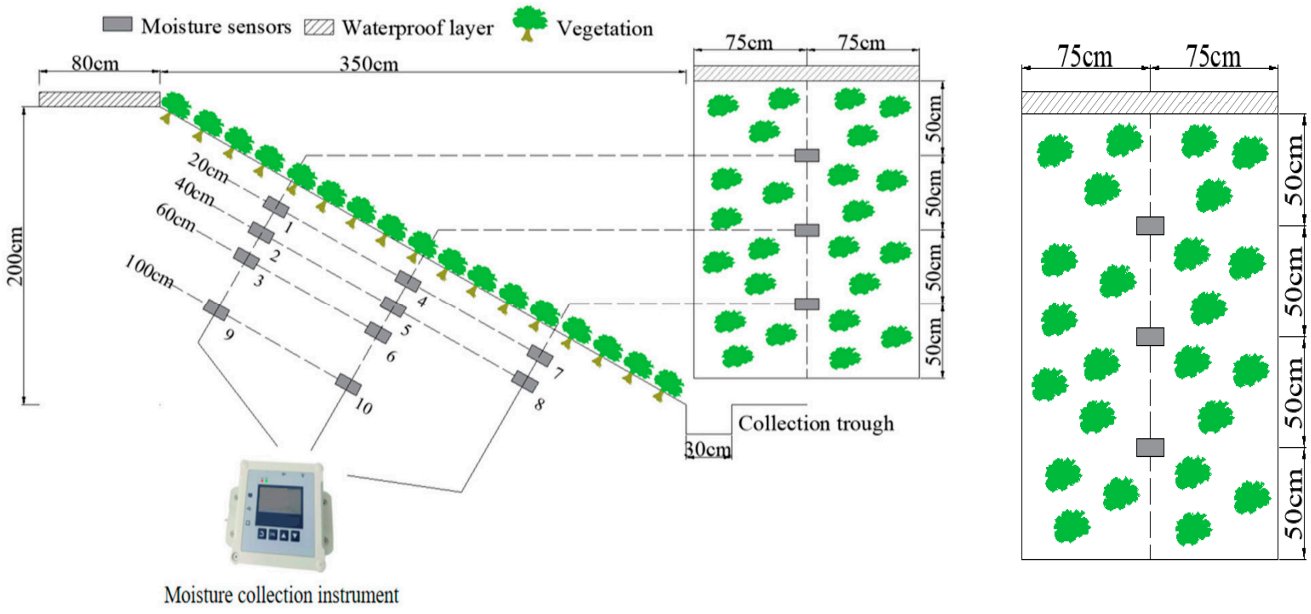

Figure 4. Schematic diagram of the slope model; (**a**) cross-section; (**b**) front view.

2.4. Vegetation Cultivation

Wuhan, Hubei belongs to a subtropical monsoon climate characterized by distinct seasons and abundant rainfall. Due to these characteristics, cynodon dactylon and magnolia multiflora have become commonly used dominant herbaceous and shrub species in the region. Cynodon dactylon is effective in slope protection. Magnolia multiflora is an excellent soil and water conservation shrub. Its developed root system can retain water and stabilize soil, and its stems and leaves can resist rainwater erosion on slopes. Therefore, this experiment selected cynodon dactylon and magnolia multiflora as the slope protection vegetation [15,31].

The selected planting density is 6.5 g/m^2, and the seeding quantity for each slope amounts to 39 g. The total seeding amount for the mixed planting of cynodon dactylon and magnolia multiflora on the slope is 39 g (usage ratio of 1:5 between cynodon dactylon and magnolia multiflora). Prior to seeding, uniformly moisten the slope surface to ensure

thorough soil saturation. After determining the seed quantity, sow accordingly and overlay the slope surface with a layer of fine soil approximately 2–4 mm thick. Subsequently, the fine soil layer was watered to thoroughly moisten it and create a unified surface. Water and apply nutrient solution regularly to stimulate vegetation growth. Record the average vegetation height and coverage every 7 days, as shown in Figure 5, 70 day vegetation growth as shown in Figure 6. The average plant height was measured as the vertical distance from the lowest point of the rootstock to the top of the stems and leaves. During each sampling event, several plants were randomly selected within the designated area. Their stems were straightened, and a steel tape measure was used to take the measurements. The maximum and minimum values were excluded, and the mean of the remaining data was taken as the average plant height. Vegetation coverage was evaluated as the ratio of the total vertical projection area of all plants in a given area to the area's total size. In practice, a custom-made cardboard frame measuring 0.1 m by 0.1 m and divided into 0.01 m intervals was placed at predefined sampling points. A fine needle was inserted vertically into each vertex of the grid from top to bottom and from left to right. When the needle touched vegetation, the point was recorded as "present". It should be noted that the four types of slopes described in the text were constructed using the soil physical properties presented in Table 1.

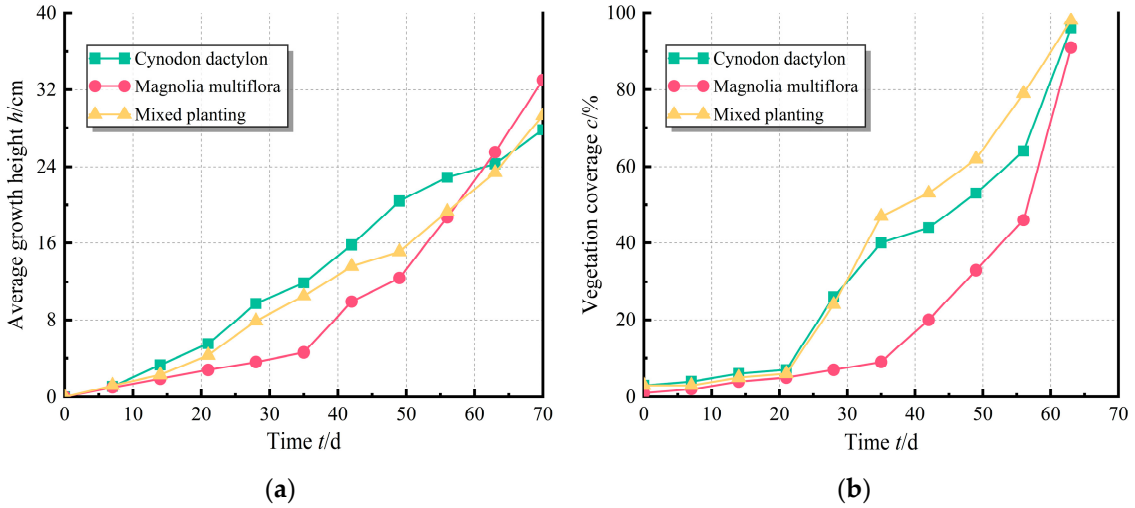

Figure 5. Vegetation growth record; (**a**) average vegetation height; (**b**) vegetation coverage.

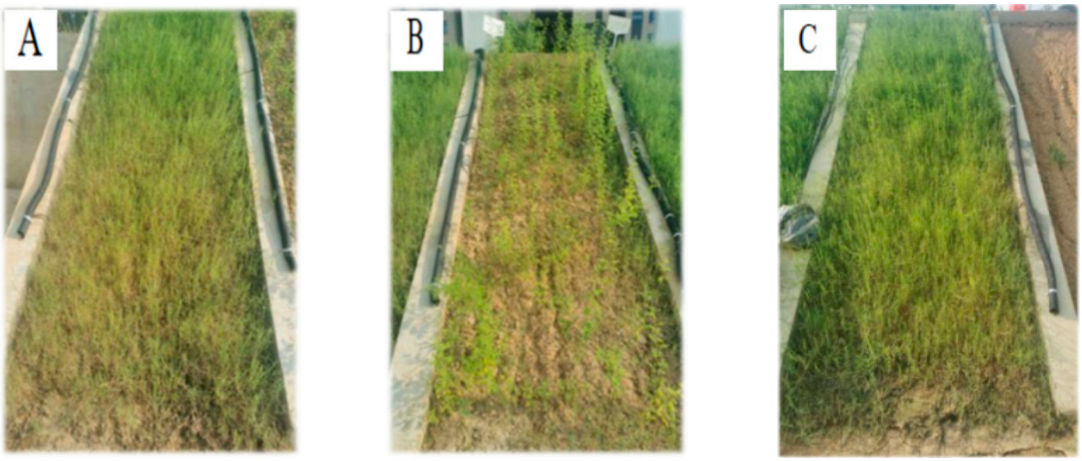

Figure 6. Growth chart of vegetation at 70 days; (**A**) cynodon dactylon; (**B**) magnolia multiflora; (**C**) mixed planting.

3. Test Results and Analysis

From 19 to 20 September 2021, the slope experimental site experienced a natural rainfall event lasting a total of 9 h, with a cumulative rainfall of 40.5 mm. Data from this period were selected for analysis. Since no significant change occurred in deeper soil layers, only 0.2 m and 0.4 m deep soil layers were analyzed, so as to study the spatiotemporal response of soil water content under natural rainfall conditions.

3.1. Empirical Patterns of Spatiotemporal Variation in Slope Moisture Content

As shown in Figure 7, in the bare slope, from 1 h to 5 h of rainfall, there is a noticeable increase in moisture content within the 0.2 m soil layer across all areas, while the 0.4 m soil layer shows minimal change. This suggests that without vegetation protection, rainwater is primarily partitioned into infiltration within the 0.2 m soil layer and surface runoff along the slope.

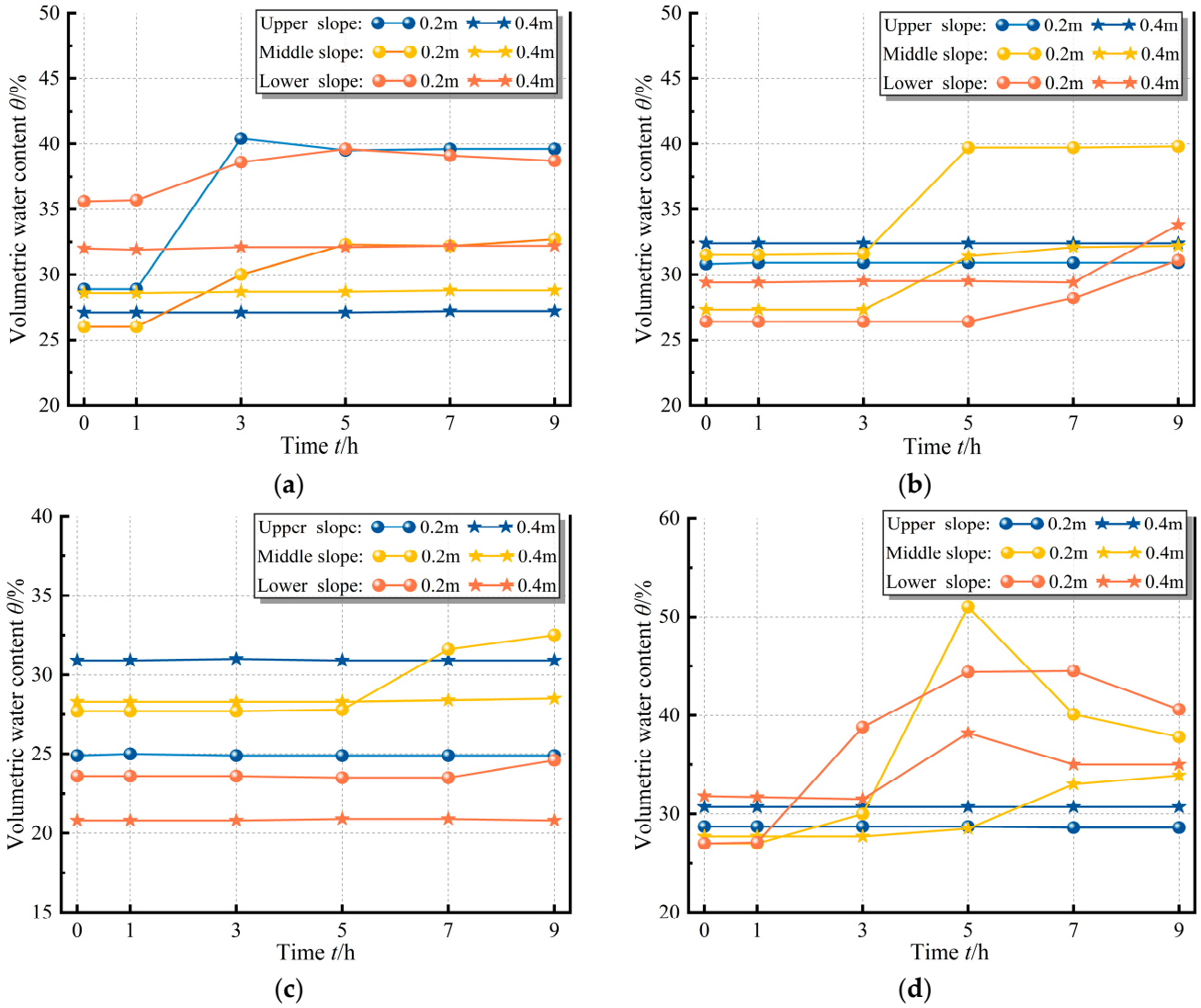

Figure 7. Temporal and spatial variations in moisture content in different soil layers; (**a**) bare; (**b**) herbaceous; (**c**) shrub; (**d**) mixed.

In the herbaceous slope, during the first 3 h, there is no significant change in water content at depths of 0.2 m and 0.4 m. This suggests that vegetation interception delays the infiltration of rainwater to the slope surface. From 3 to 5 h, the mid-slope regions exhibit consistent increase in soil moisture content. From 5 h and 9 h, the rate of moisture

increase decelerates at the 0.2 m and 0.4 m depths in mid-slope areas, whereas the lower slope regions begin to show rising moisture levels. As the mid-slope soil nears saturation moisture content, water gradually infiltrates toward the lower slope regions.

In the shrub slope, soil moisture content remains relatively stable across all soil layers during the first 5 h. During the period from 5 h to 7 h, soil moisture content at a depth of 0.2 m within the mid-slope region experiences a slight increase. From 7 h to 9 h, the rate of soil moisture increase within the 0.2 m soil layer in the mid-slope region decreases, while there is a marginal rise in moisture content in the lower slope regions of this layer. This pattern aligns with the trends observed in the herbaceous slope, but the change range of shrub slope is small. The predominant factor is the relatively weaker rainfall interception capacity of the magnolia multiflora canopy, leading to reduced rainfall interception and increased surface runoff.

During the first hour, moisture content remains constant across all soil layers in the mixed vegetation slope. Between 1 h and 5 h, the 0.2 m soil layer in the mid-slope region shows a significantly higher increase rate than the 0.4 m layer. Additionally, soil moisture in the lower slope areas approaches saturation. From 5 h to 9 h, moisture content declines noticeably within the 0.2 m soil layer in the mid-slope region, while showing a consistent upward trend in the 0.4 m soil layer. Meanwhile, soil moisture in the lower slope regions experiences a declining trend.

3.2. Empirical Patterns of Infiltration Rate and Cumulative Infiltration on Slope

The rainfall infiltration rate refers to the rate at which the rainfall amount per unit area enters the soil within a unit of time, typically reflecting the soil's water infiltration capacity [32]. It is calculated by:

$$\mathrm{V} = \frac{\Delta\omega}{\Delta t} \times \frac{V_t}{A_c} \quad (1)$$

where $\Delta\omega$ is the change in volumetric moisture content from the initial value (%), Δt is the time interval (h), A_c is the effective rain-receiving area of the slope (m^2), V_t is the volume of soil within the sensor measurement range (m^3).

Cumulative rainfall infiltration refers to the total volume of rainwater that successfully penetrates the ground surface and enters the slope soil mass during a rainfall event. It is derived by integrating the infiltration rate curve over the specified time interval [33,34].

As shown in Figure 8, the highest infiltration rates for each type of slope occur at a burial depth of 0.2 m. Specifically, the maximum rates are measured as 2.938×10^{-2} m/h for the bare slope, 1.841×10^{-2} m/h for the herbaceous slope, 0.914×10^{-2} m/h for the shrub slope, and 5.821×10^{-2} m/h for the mixed slope. Moreover, as the burial depth increases, the infiltration rates of all types of slopes show a decreasing trend.

In the 0.2 m soil layer, the herbaceous slope exhibits a lower infiltration rate than the bare slope, while in the 0.4, 0.6, and 1.0 m soil layers, it is higher than that of the bare slope. As shown in Figure 9, the cumulative infiltration of herbaceous slope is greater than that of bare slope, with an increase of 21.32%, This reflects the positive influence of cynodon dactylon on increasing rainwater infiltration. For the shrub slope, the 0.2 m layer shows lower infiltration than the bare slope, but no significant difference occurs at deeper layers (0.4–1.0 m). Its cumulative infiltration is 61.06% lower than the bare slope's. This indicates that the multiflora rose has suppressed rainwater infiltration. The mixed slope surpasses the other three types at 0.2 m depth, with little divergence from the herbaceous slope below this depth. The mixed vegetation enhances infiltration capacity by 77.07%. This demonstrates that mixed vegetation enhances rainwater infiltration and that this effect is stronger than that of cynodon dactylon.

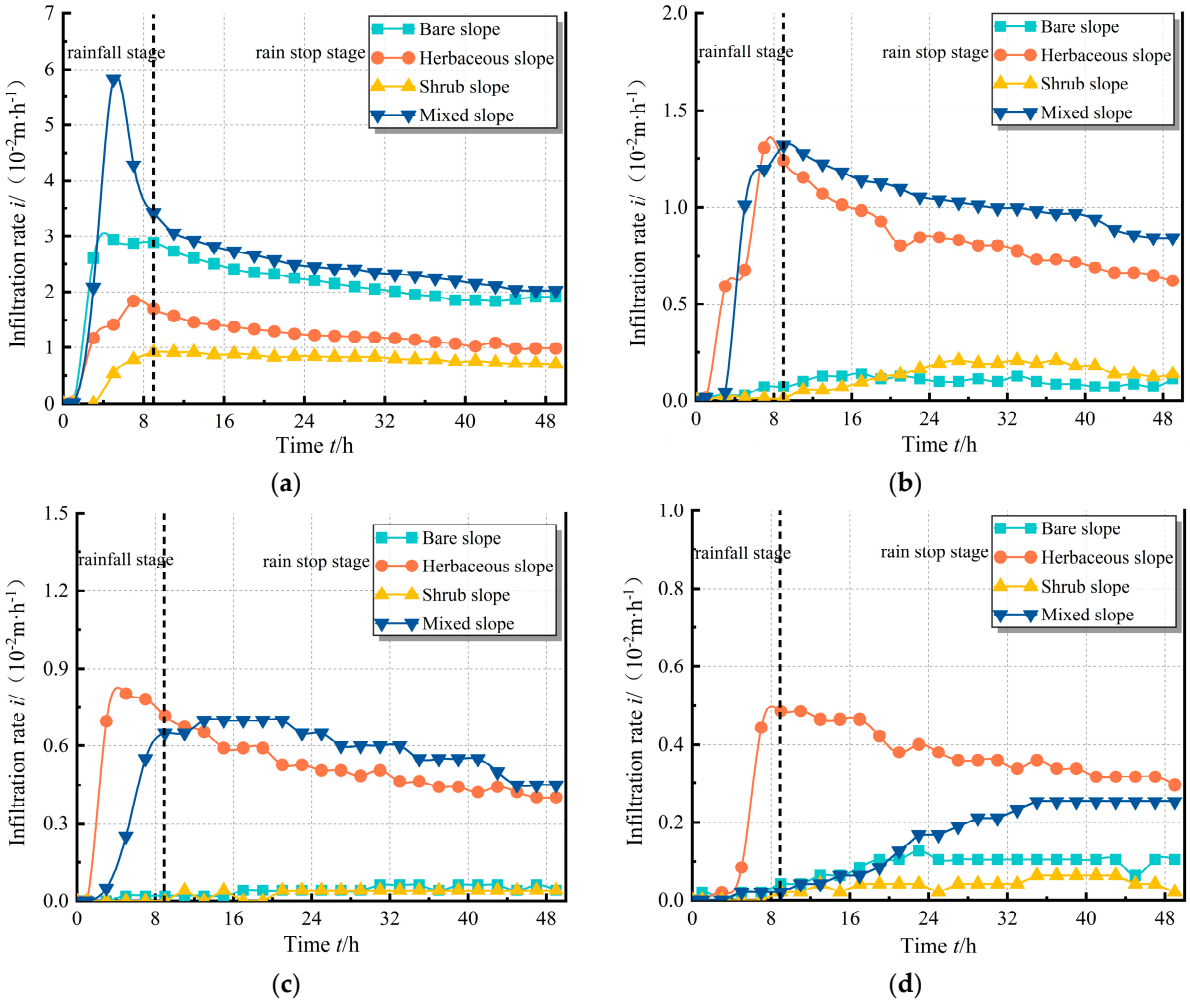

Figure 8. Temporal variations in infiltration rates at different burial depths; (**a**) 0.2 m; (**b**) 0.4 m; (**c**) 0.6 m; (**d**) 1.0 m.

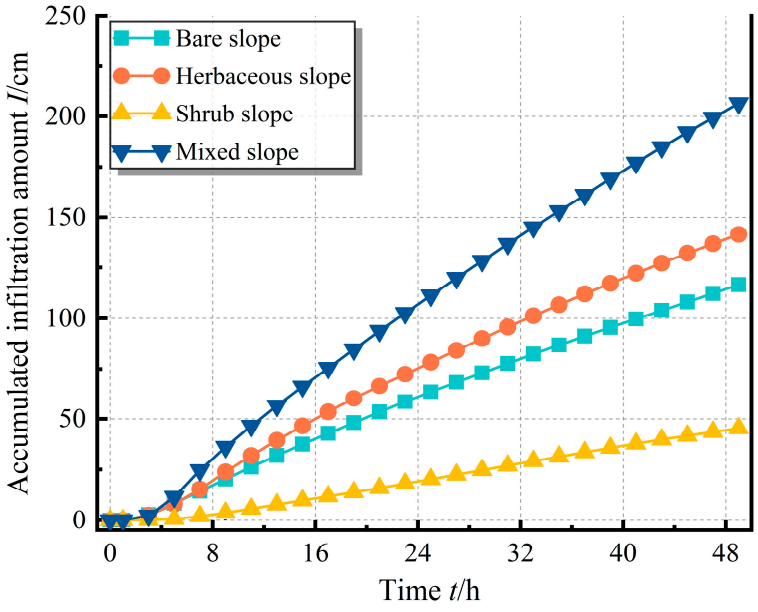

Figure 9. Variation in cumulative rainfall infiltration over time.

4. Strength and Hydraulic Properties of Unsaturated Rooted Soil

4.1. Materials and Methods

To characterize the hydro-mechanical properties of the soil, key parameters including the soil-water characteristic curve (SWCC), permeability coefficient, and shear strength parameters were obtained experimentally. These parameters are critical inputs for the subsequent numerical simulation studies. Figure 10 illustrates the instruments and equipment used for measuring these three indicators. Among them, the soil-water characteristic curve test and the permeability test were conducted using the GCTS Fredlund pressure plate apparatus produced by Shuangjiete Technology (Beijing, China) company and the double-cell falling-head automatic permeameter manufactured by Tuoce (Suzhou, China) company. The shear test was performed using the HC-UDR-300 triple unsaturated soil direct shear apparatus produced by Suzhou Huicai Technology (Kunshan, China) company, which allows for the independent application of matric suction and shear stress.

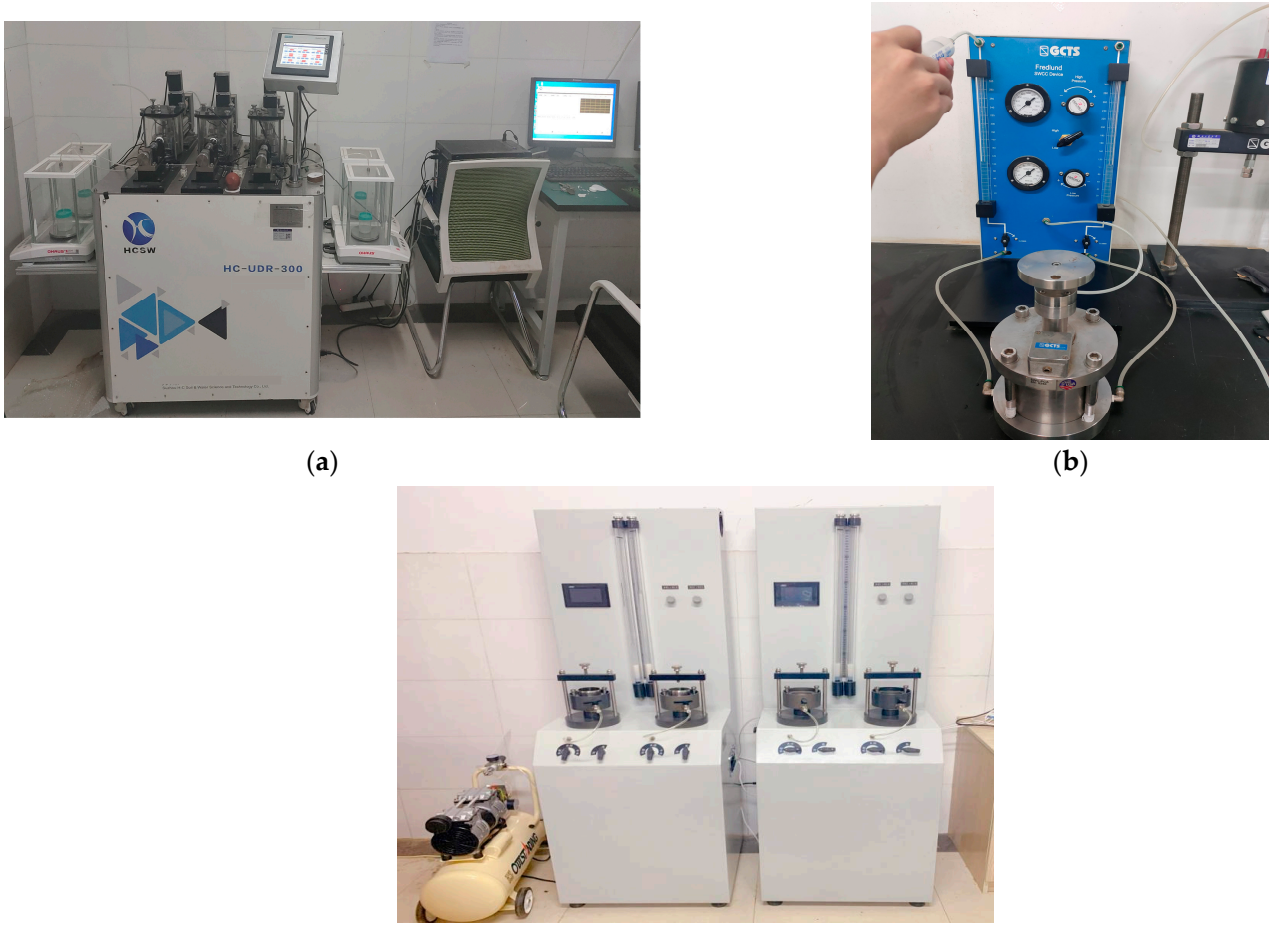

(**a**) (**b**)

(**c**)

Figure 10. Experimental apparatus; (**a**) triple direct shear apparatus; (**b**) fredlund SWCC device; (**c**) variable head permeameter.

The plant roots used in the experiment were taken from plants grown under the same conditions and at the same time as the slope models. Insert ring knives into three different positions in the cynodon dactylon pot. The mass of cynodon dactylon roots extracted from the three ring knives is averaged, yielding a root mass of 0.2 g, and the root length of cynodon dactylon is 15 cm. On the shrub slope, the average spacing between magnolia multiflora plants is measured to be 25 cm. After excavating the root system from the magnolia multiflora planting pot, the average length and diameter of the roots

are determined to be 50 cm and 5.3 mm, respectively. The volumetric cylinder method is employed to measure the volume of magnolia multiflora plant roots. Comparing this volume with that of the growing soil, the root inclusion rate of magnolia multiflora is determined to be 0.085%. This corresponds to 5 roots, each measuring 2 cm in length, within the ring knives. Based on the root mass ratios between herbaceous slope and mixed slope for cynodon dactylon, and between shrub slope and mixed slope for magnolia multiflora, the respective root biomass contributions of both species in the mixed soil system were determined. Instructions for the production process of a ring knife sample containing root soil: The root system of cynodon dactylon was mixed evenly with a prepared soil sample and poured into a sample maker, then compacted with a jack. The root system of magnolia multiflora was cut into a length of 2 cm with scissors, inserted into the soil sample of the sample maker by hand, and finally compacted with a jack. The arrangement of the root system must ensure uniform distribution within the ring knife. To ensure that the compactness of the samples matched that of the slope model, ring-knife samples with dry density of 1.5 g/cm^3 were prepared, the diameter is 61.8 mm and the height is 2 cm, with quality moisture contents of 16%, 18%, 20%, 22%, 24%, 26%, as shown in Figure 11. Set the shear loading rate to 0.8 mm/min through the computer, with a final shear displacement of 6 mm and an axial loading rate of 1 mm/min.

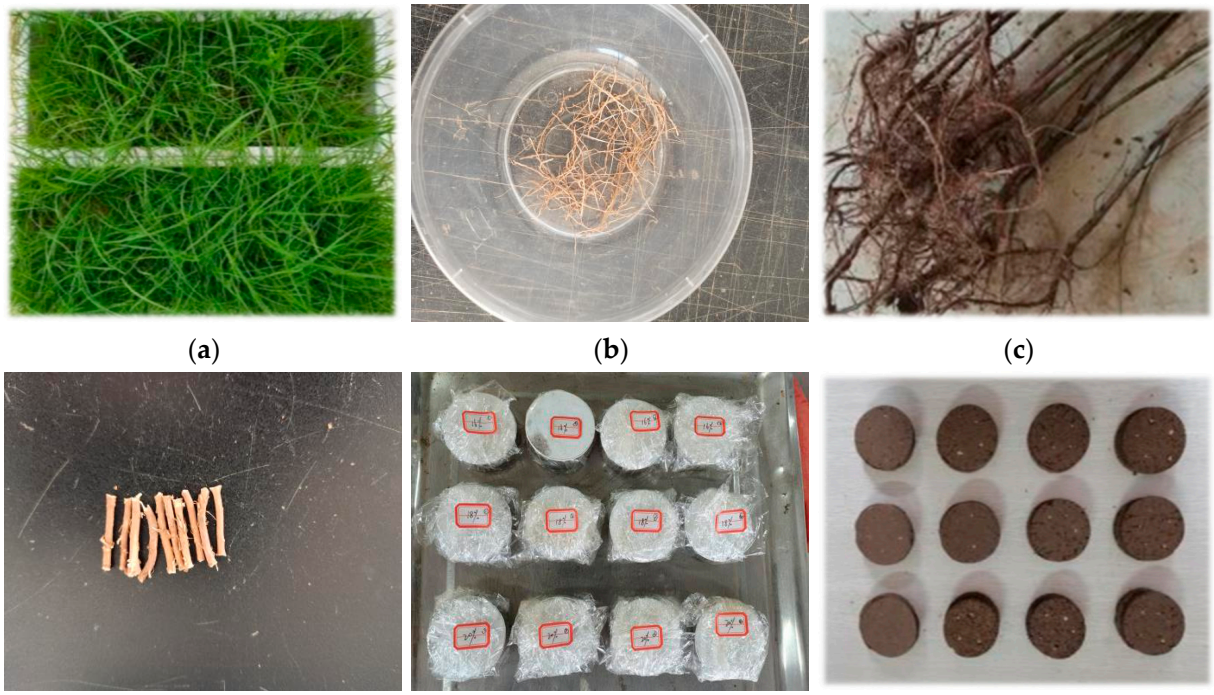

Figure 11. Soil sample preparation; (**a**) cynodon dactylon pot; (**b**) roots of cynodon dactylon; (**c**) excavated magnolia multiflora; (**d**) roots of magnolia multiflora; (**e**) ring knife soil sample; (**f**) damaged soil sample.

Utilizing the VG model proposed by Van Genuchten to fit the soil water characteristic curve and obtain the corresponding parameters [35], the VG model is as follows:

$$\theta = \theta_r + \frac{\theta_s - \theta_r}{\left[1 + (a\Psi)^n\right]^m} \quad (2)$$

where θ represents the variable of soil volume moisture content (%); θ_r represents residual moisture content (%); θ_s represents saturated moisture content (%); a, m and n are parameters, $m = 1 - 1/n$; Ψ represents the value of air-entry suction.

The permeability coefficient of the soil sample is obtained according to the following formula:

$$K_T = 2.3 \frac{aL}{A(t_2 - t_1)} \log \frac{H_1}{H_2} \quad (3)$$

where 2.3 is a unitless conversion coefficient between natural logarithms and common logarithms; a denotes the cross-sectional area of the water head tube (cm^2); L represents the height of the seepage path (cm); A indicates the cross-sectional area of the ring-knife sample (cm^2), $t_2 - t_1$ represents the time interval (s), H_1 and H_2 represent the initial water head and the final water head (mm).

The permeability coefficient at a water temperature of 20 °C was converted using the following formula:

$$K_{20} = K_T \frac{\eta_T}{\eta_{20}} \quad (4)$$

where K_T and K_{20} represent the permeability coefficients of the soil sample at water temperatures of T °C and 20 °C (cm/s), η_T and η_{20} denote the dynamic viscosity coefficients of water at temperatures T °C and 20 °C.

The measured cross-sectional area of the water head tube was 0.562 cm^2, the cross-sectional area of the ring-specimen was 30 cm^2, the seepage path is 4 cm, and the time difference is 5 s.

4.2. Results

Figure 12 illustrates the relationship between shear strength and normal stress of soil samples with different moisture contents. The shear strength exhibits a significant positive correlation with normal stress but decreases markedly with increasing water content. According to the Mohr-Coulomb shear strength formula, the shear strength of soil is primarily determined by cohesion c and the internal friction angle φ. After linear fitting of Figure 12, the slope and intercept of the obtained line represent the internal friction angle and cohesion of the soil sample, respectively, as shown in Figure 13. Under different moisture content conditions, the internal friction angle and cohesion of the four soil samples decrease with increasing moisture content. When the moisture content is the same, the order of cohesion and internal friction angle is as follows: mixed > magnolia multiflora > cynodon dactylon > bare. Soil with roots shows a more noticeable increase in cohesion at higher moisture content levels compared to bare soil. However, the increase in internal friction angle is not as significant [36–38].

The soil-water characteristic curves for different soils with roots and the fitted parameters of the Van Genuchten (VG) model are shown in Figure 14 and Table 3, respectively. The permeability coefficients are presented in Table 4.

Table 3. Parameters fitted by VG model.

Root Soil Type	Scale Parameter	Fitting Parameter	Shape Parameter
	a (kPa^{-1})	m	n
Bare	50.40	0.395	1.653
Cynodon dactylon	48.90	0.375	1.600
Magnolia multiflora	45.56	0.388	1.635
Mixed	46.51	0.403	1.674

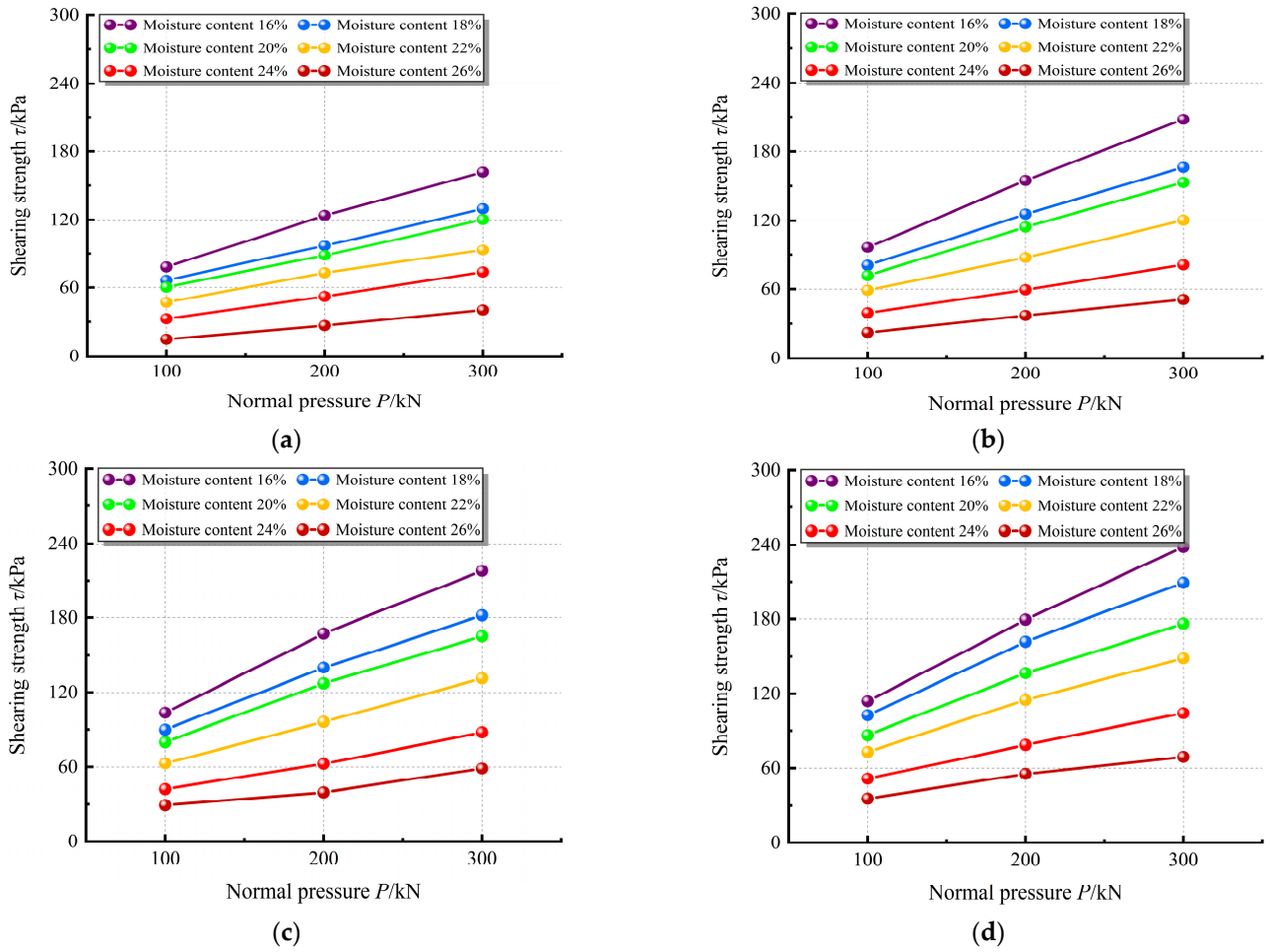

Figure 12. Variation in soil shear strength with moisture content and normal pressure (soil type: loam; dry density: 1.5 g/cm^3); (**a**) bare; (**b**) cynodon dactylon; (**c**) magnolia multiflora; (**d**) mixed.

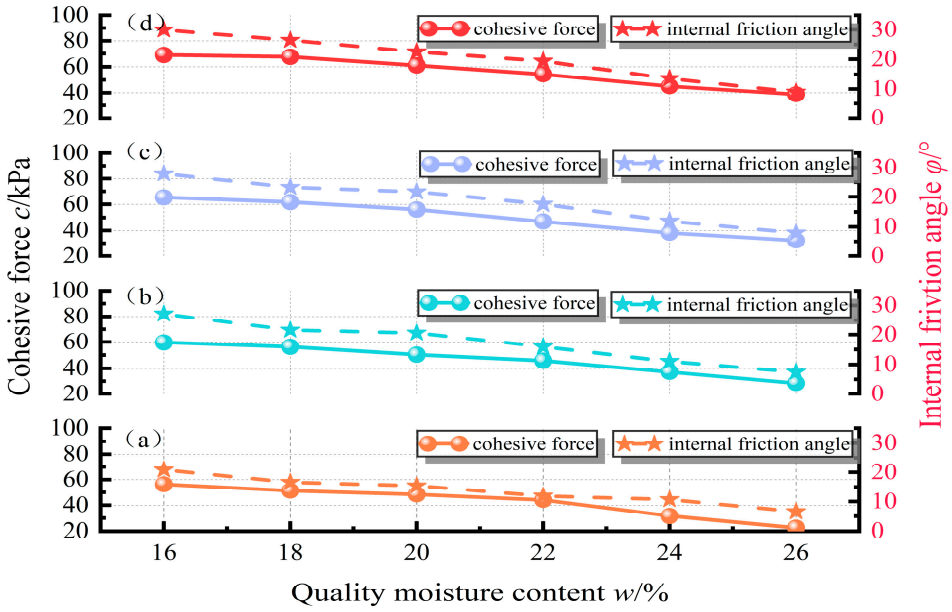

Figure 13. Variation in soil shear strength parameters with moisture content (soil type: loam; dry density: 1.5 g/cm^3); (**a**) bare; (**b**) cynodon dactylon; (**c**) magnolia multiflora; (**d**) mixed.

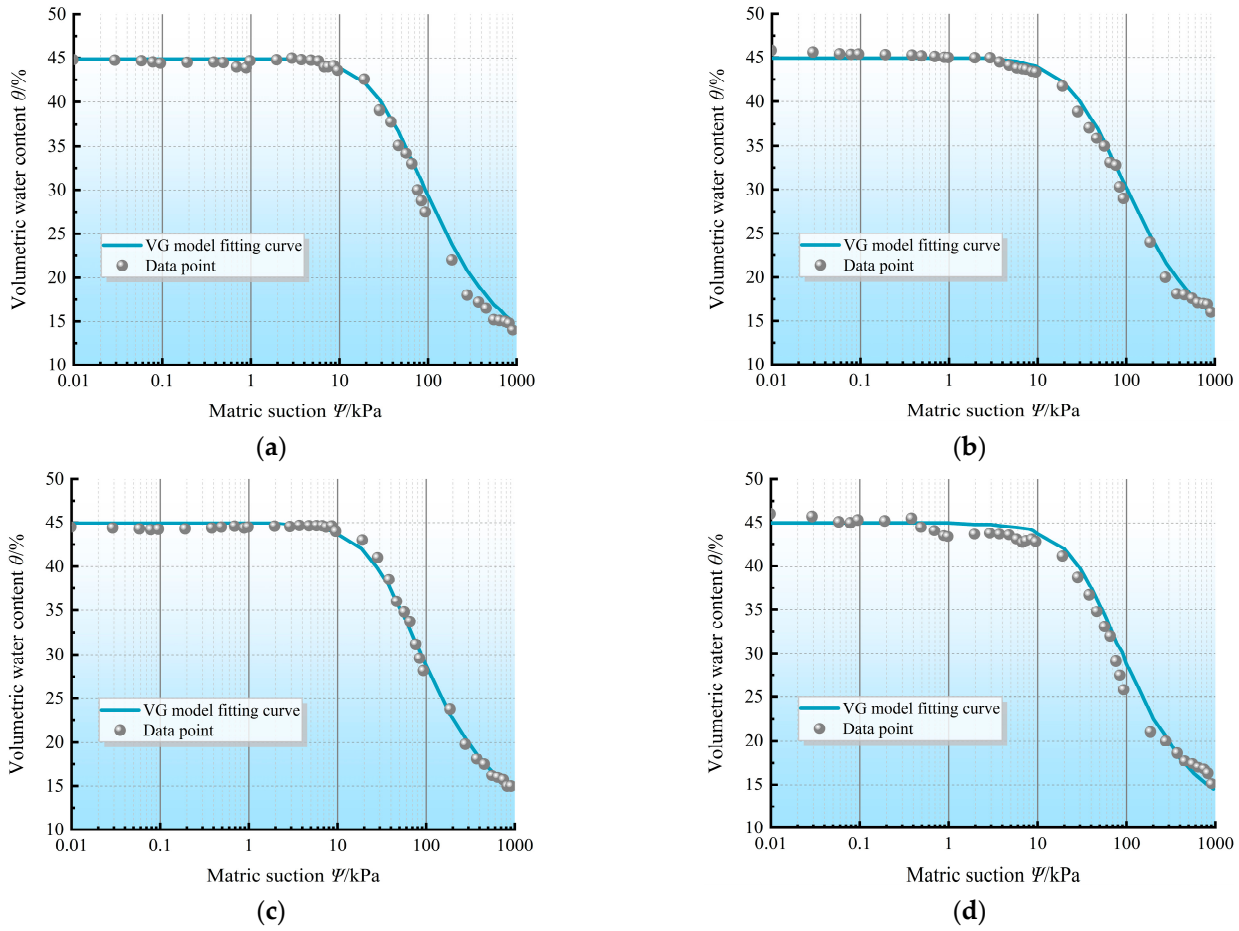

Figure 14. Fitting of SWCC with VG model; (**a**) bare; (**b**) cynodon dactylon; (**c**) magnolia multiflora; (**d**) mixed.

Table 4. Permeability coefficient at saturation.

Root Soil Type	Bare	Cynodon Dactylon	Magnolia Multiflora	Mixed
SHC (cm/s)	2.47×10^{-4}	4.37×10^{-4}	4.46×10^{-4}	4.77×10^{-4}

5. Stability Analysis of Slope Protected by Different Vegetation

5.1. Reliability Evaluation of Numerical Simulation—Model Establishment

Numerical simulation simulates the different behaviors of slopes under various events by establishing numerical models. Once the simulated behaviors can reproduce the behaviors observed from field experiments, this numerical model can be considered validated [39]. The numerical simulations were conducted using Geostudio 2021.1 software developed by Seequent Limited, with the seep/w module employed to validate the reliability of the numerical modeling.

A seepage analysis model was established based on actual dimensions (the mixed slope was selected as the representative case due to the highest complexity of its computational model), as illustrated in Figure 15. The slope was divided into three primary zones: upper, middle, and lower slopes. Each zone was further subdivided according to the positions of moisture sensors and the depth of vegetation root influence, with relevant parameters assigned, including soil-water characteristic curves, initial moisture content, and hydraulic conductivity. The root influence zones of cynodon dactylon and magnolia multiflora extended vertically to depths of 0.15 m and 0.5 m below the slope surface. The average

rainfall intensity was applied as the flow boundary condition on the slope surface. The analysis type was set to transient seepage. Impermeable boundaries are established at the top and bottom of the slope. Based on actual rainfall conditions, the rainfall boundary condition is set to 4.5 mm/h for a duration of 9 h, each calculation step takes 1 h, and the grid was divided into quadrilateral squares with a size of 5 cm, comprising 2168 nodes and 2074 elements. The reliability of the model was verified by comparing the simulated moisture content values with real-time monitoring values [40,41].

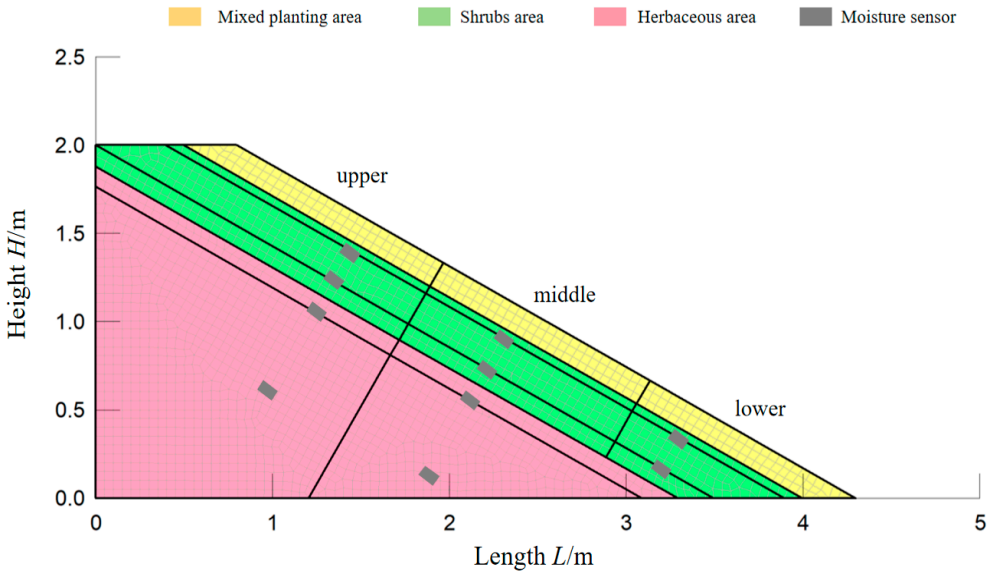

Figure 15. Seepage analysis numerical model.

5.2. Results Analysis

Figure 16 presents a comparative analysis of the measured and simulated volumetric water content values obtained from multiple sensor points installed at different burial depths within mixed slope under sustained rainfall conditions. It can be observed that the discrepancies between the measured and simulated values are relatively small and fall within an acceptable margin of error. More importantly, both datasets exhibit consistent temporal variations and distribution trends, indicating that the model accurately captures the hydrological processes. Given the close agreement between the observed and simulated results, the potential deviation introduced into subsequent slope stability analysis is considered negligible. These results collectively demonstrate the fundamental reliability of the numerical model in simulating water movement within vegetated slope systems under rainfall infiltration conditions.

5.3. Stability Analysis of Slope Protected by Different Vegetation—Model Establishment

Based on the seepage analysis results, numerical analysis was carried out using the slope/w module in Geo-studio to assess the stability of slopes protected by various vegetation types. The safety factor was calculated using the Morgenstern-Price method within the limit equilibrium framework, with the Mohr-Coulomb strength criterion serving as the theoretical basis [42]. The boundary range has a certain impact on the accuracy of calculations when using finite element analysis for slope models. Therefore, to adjust for this, the slope model was proportionally scaled up by five times [43]. The division of the stability calculation model is shown in Figure 17.

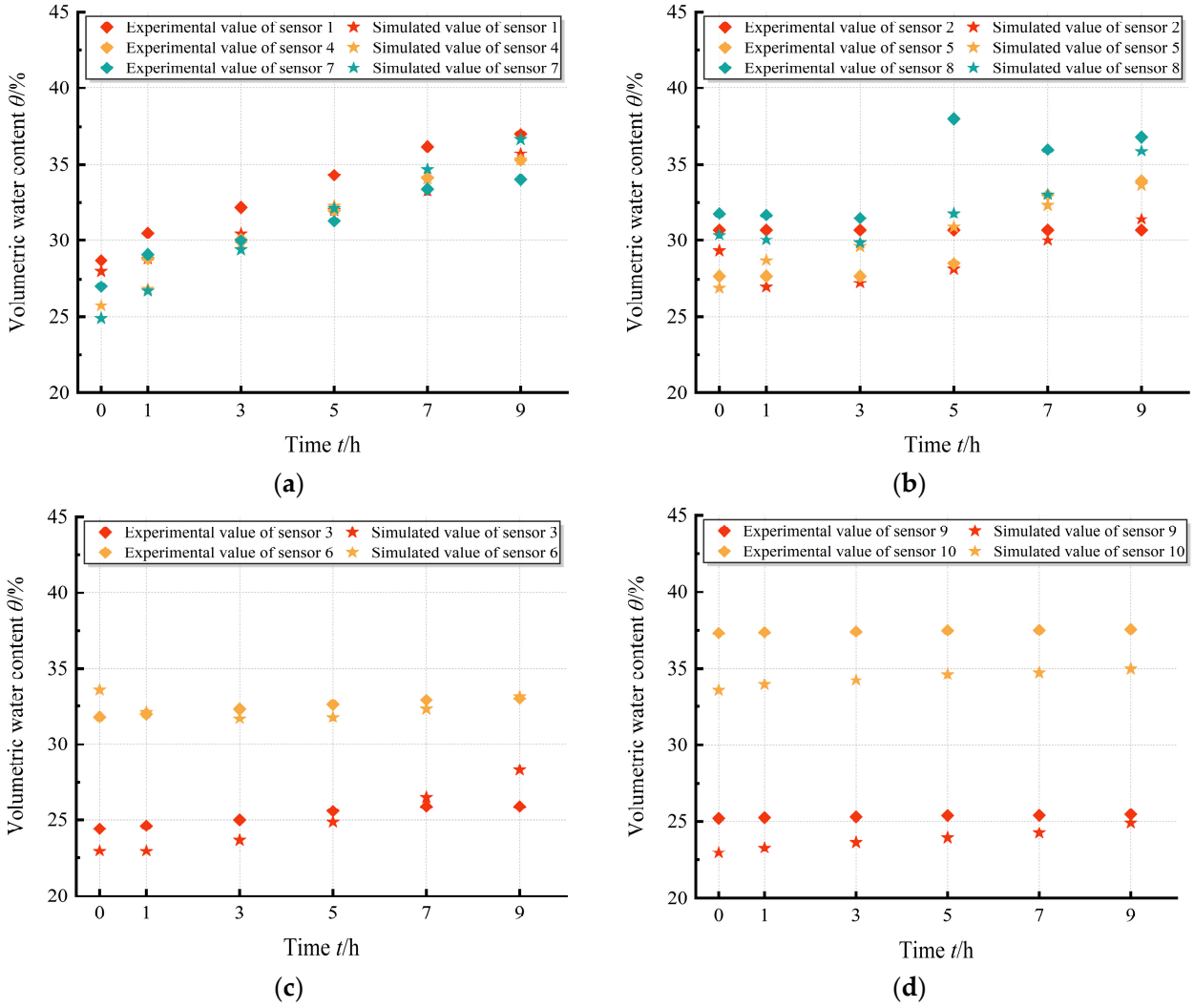

Figure 16. Measured and simulated water content for monitoring points at different depths; (**a**) 0.2 m; (**b**) 0.4 m; (**c**) 0.6 m; (**d**) 1.0 m.

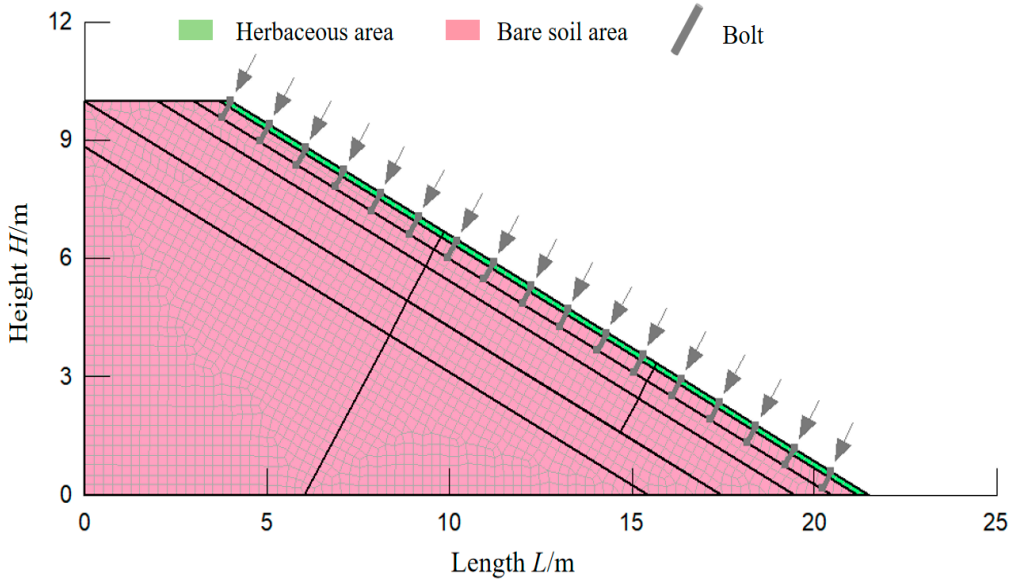

Figure 17. Stability analysis numerical model.

Linear regression was performed on the relationship between shear strength parameters and volumetric moisture content, as shown in Table 5. Subsequently, cohesion and internal friction angle were assigned to different regions according to the initial moisture content. Due to the small diameter and high density of cynodon dactylon roots, the zone within 0.15 m below the slope surface of the herbaceous slope was simplified as a cynodon dactylon root-soil composite, with its strength parameters are assigned based on the moisture content. In contrast, magnolia multiflora, being a shrub species with larger root diameters and lower density, primarily reinforces the slope through the anchoring force provided by its robust root system, Since it is extremely difficult to accurately simulate the mechanical equivalence of magnolia multiflora root systems, the method of simplifying magnolia multiflora roots into anchor rods is adopted to approximately reproduce their reinforcing effects on slopes. Therefore, the region within 0.5 m below the slope surface of the shrub slope was modeled using anchor rods embedded at 1.2 m intervals, assigned with tensile strength and pullout resistance, and the shear strength parameters of the soil were still assigned based on the values for bare soil. Within the mixed slope, the soil layer extending 0.15 m below the slope surface is represented as a cynodon dactylon root-soil composite, while the magnolia multiflora roots within the soil layer extending 0.5 m below the slope surface are simplified as anchor rods [44–46].

Table 5. Linear equation of shear strength parameters and moisture content.

Root Soil Type	Cohesion c/kPa	Internal Friction Angle φ/°
bare	$y = -221.45x + 112.14$	$y = -88.57x + 41.57$
cynodon dactylon	$y = -208.47x + 111.93$	$y = -128.11x + 57.64$
magnolia multiflora	$y = -234.29x + 123.87$	$y = -131.39x + 59.77$
mixed	$y = -214.93x + 123.66$	$y = -139.94x + 64.22$

To fully assess the long-term stability of the slope, the rainfall duration was set to 112 h with stability calculations conducted at 8 h intervals, resulting in 15 calculation steps. Many scholars have used limit equilibrium method to investigate slope's stability [47]. However, the shear strength parameters of rooted soil was treated as a constant value [5,19,27]. The soil shear strength parameters undergo weakening under water influence, neglecting this effect can overestimate slope stability [48]. Hence, in order to accurately evaluate slope's stability, a technique of gradually assigning shear strength parameters and individually computing the slope's stability at each stage was implemented. Firstly, the seep/w module was utilized to simulate the infiltration of rainfall and obtain the variation in volumetric water content at each monitoring point within the slope. Subsequently, the corresponding shear strength parameters for each monitoring point at each stage were calculated based on Table 5. Finally, the shear strength parameters were incrementally assigned step by step in the slope/w.

It should be noted that the stability analysis is based on the spatiotemporal variation in moisture content rather than direct measurement of pore water pressure or matric suction, representing a simplified approach [28,48].

5.4. Results Analysis

The slope stability shows a notable correlation with rainfall duration, showing an overall decreasing trend in safety factor during rainfall, as shown in Figure 18. The safety factor of the bare slope is consistently lower than that of the vegetated slopes. Before rainfall, the shrub slope exhibited the highest safety factor, reaching 3.046, followed by the mixed slope (2.948) and the herbaceous slope (2.81). Compared to the bare soil slope's

safety factor of 2.766, these values represent increases of 0.28, 0.182, and 0.044, respectively. After rainfall, the mixed slope demonstrated the highest safety factor at 1.361, followed by the shrub slope (1.275) and the herbaceous slope (1.192). Compared to the bare soil slope's safety factor of 1.139, these values correspond to improvements of 0.222, 0.136, and 0.053, respectively.

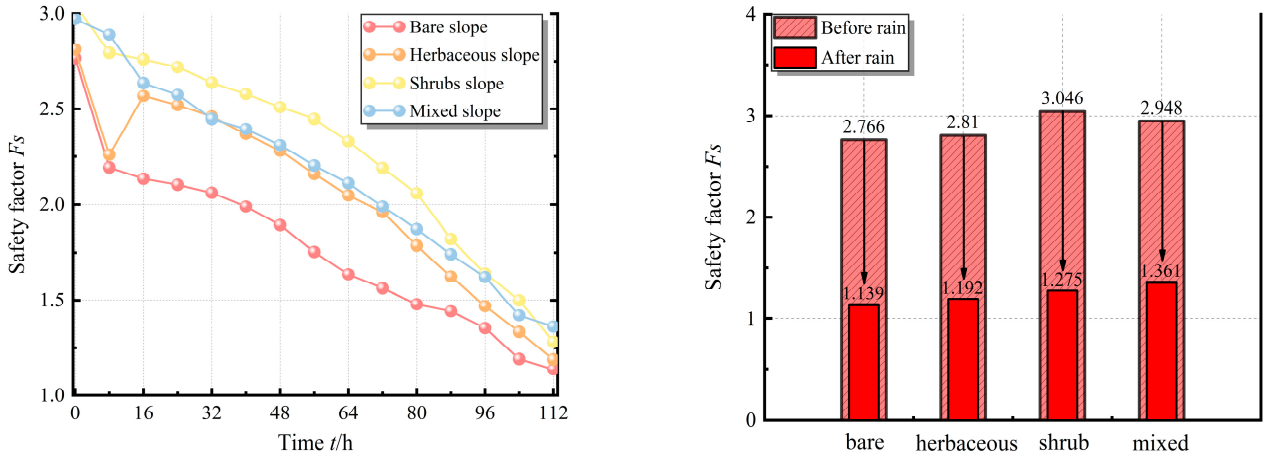

Figure 18. SF Changes with rainfall; (**a**) variation in SF; (**b**) SF before and after rainfall.

The initial moisture content of the shrub slope averaged 27.96%, while that of the mixed slope averaged 29.16%. Owing to its lower initial moisture content, the shrub slope exhibited higher shear strength parameters than the mixed slope. This accounts for the shrub slope's superior safety factor prior to rainfall. As the rainfall continued, the moisture content within the slope gradually approached saturation. The difference in moisture content between the slopes diminished, leading to the safety factor of the mixed slope gradually surpassing that of the shrub slope. Therefore, under the experimental conditions, the trends and relative performance of the safety factor improvements by herbaceous, shrubs, and mixed vegetation generally followed the order of mixed > shrub > herbaceous, which is largely consistent with the conclusions drawn from the shear tests.

The system identified a total of 405 distinct slip surfaces through computational analysis. Among these, the slip surface associated with the minimum safety factor is considered the critical slip surface. In Figure 19, the critical slip surface is represented by the white arc, the corresponding safety factor value is marked by the red dot, and R denotes the radius of the slip surface. It is observed that the position of the critical slip surface varies significantly before and after rainfall events. As rainfall progresses, rainwater initially infiltrates the shallow soil layers, resulting in increased moisture content and a consequent reduction in shear strength due to matric suction loss and soil softening. This degradation of near-surface soil properties reduces slope stability and causes the critical slip surface to migrate from a deeper position under pre-rainfall conditions to a shallower depth following rainfall infiltration.

In summary, under rainfall conditions, slope stability gradually weakens primarily due to the increase in moisture content within the slopes, leading to a decrease in shear strength. Vegetated slopes exhibit stronger stability than the bare slope, because the presence of roots increases the shear strength of the soil [49,50]. When the moisture content is higher, the cohesion of root-soil composite increases more significantly, and the increase in shear strength is mainly provided by cohesion [51]. Due to the presence of roots, the matric suction within the soil increases the shear strength of the slope soil to a greater extent in

vegetated slopes [28,52]. Furthermore, the canopy of vegetation can slow down the falling speed of rainwater, slowing down the rainfall's impact on the slope surface. After rainfall ceases, the transpiration process of vegetated soil gradually evaporates moisture from the slope, increasing matric suction and contributing to the stability of the slope [14,22].

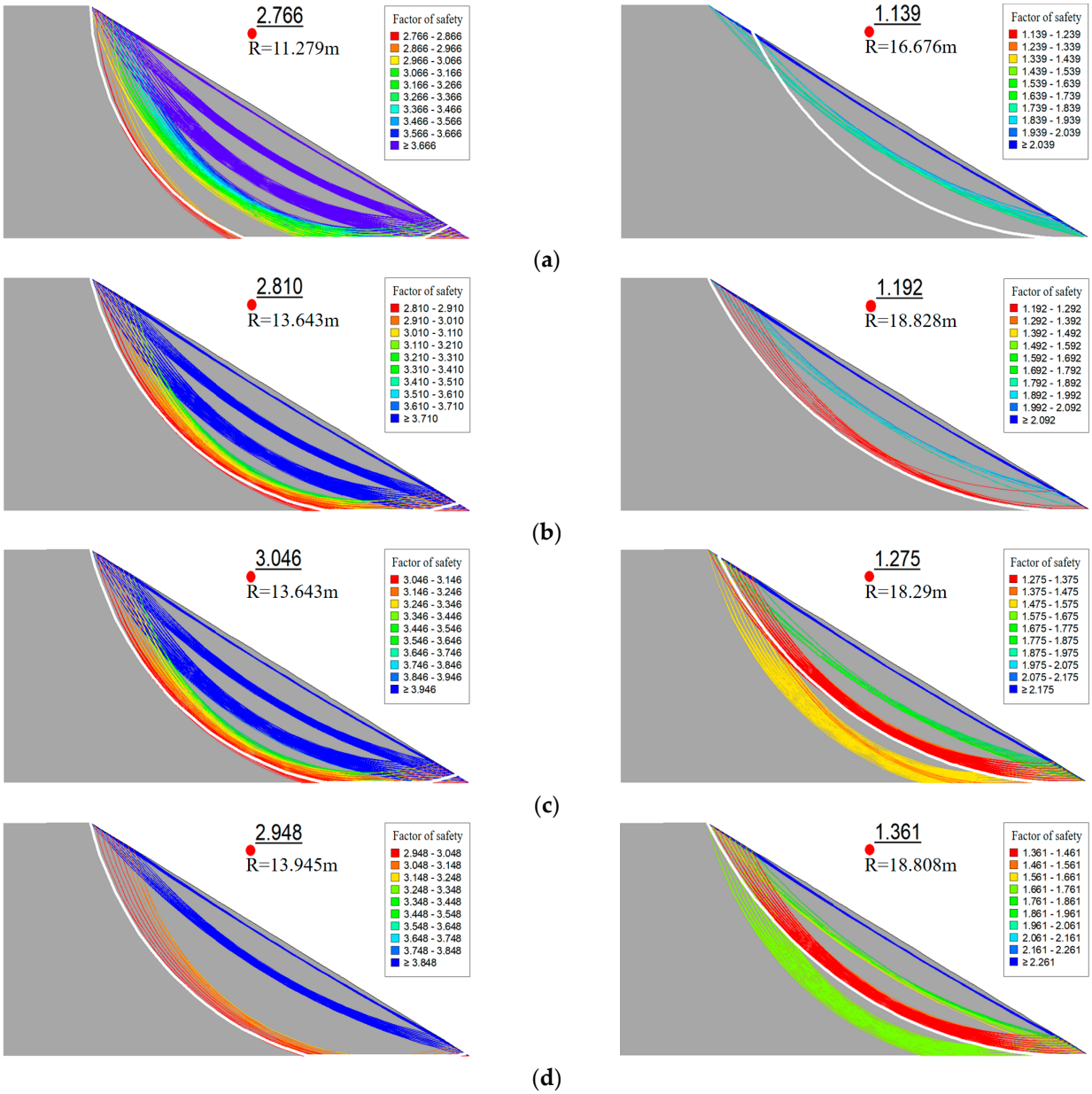

Figure 19. Cloud map of slope slip surface before and after rainfall; (**a**) bare; (**b**) herbaceous; (**c**) shrub; (**d**) mixed.

Various types of vegetation have different impacts on improving slope stability. The roots of herbaceous vegetation are shallow and fine, mainly strengthening the superficial layers of the slope, this improvement is somewhat limited. Additionally, experiments on rainfall infiltration show that the presence of cynodon dactylon roots increases the amount of water entering the slope, significantly reducing the shear strength of herbaceous slopes. In contrast, shrub vegetation, with its extensive root system, greatly improves slope stability by securing the slope. Moreover, experiments indicate that magnolia multiflora roots decrease the amount of water infiltrating the slope, resulting in higher matric suction and improved shear strength. Mixed vegetation has a more complex root system, allow-

ing roots to mobilize more soil to resist shear deformation, leading to stronger root-soil interactions. It is evident that under mixed distribution, the root reinforcement effect is more significant [53].

6. Discussion

6.1. Effects of Vegetation on Slope Rainfall Infiltration

In the bare slope, little variation in infiltration rates occurs at depths of 0.4 m and below, mainly because the lack of vegetation cover generates substantial surface runoff, thereby limiting rainfall infiltration into deeper layers.

At the 0.2 m depth, the herbaceous slope exhibits a marginally lower infiltration rate than the bare slope, which results from the dense canopy of cynodon dactylon effectively intercepting rainfall, causing partial water retention on the slope surface. However, at deeper depths, the herbaceous slope demonstrates higher infiltration rates than the bare slope. This is primarily due to the root system development and metabolic activity of cynodon dactylon, which significantly improves soil structure, thereby markedly enhancing soil permeability and porosity in the rhizosphere [52].

At 0.2 m burial depth, the shrub slope exhibits lower infiltration rates compared to both the bare and herbaceous slope. At greater depths, there is no discernible difference from the bare slope. The reason stems from the comparatively larger root diameters of shrub species, which occupy soil macropores, consequently reducing infiltration capacity and inducing hydrophobicity in the rhizosphere. Plant root systems are predominantly concentrated in shallow soil layers, with magnolia multiflora exhibiting significantly higher root density in surface horizons compared to deeper strata. This root-induced hydrophobicity is primarily manifested in the superficial slope layers, impeding vertical percolation of rainfall into deeper soil layer [54–56].

The mixed slope has a more complex canopy and root structure. Its canopy density is lower than the herbaceous slope, resulting in reduced rainwater interception capacity, and the surface runoff is less than that of the shrub slope. Compared with the slope with herbaceous and shrub planting forms, the mixed slope can make more rainwater fall to the slope, providing a prerequisite for rainwater infiltration into the slope. For the root structure under the slope, the growth and metabolism of herbaceous root in the shallow layer of the slope make the soil loose, increased the porosity of the shallow soil of the slope, and weakened hydrophobicity of the shrub. Additionally, mixed planting sites demonstrate superior growth performance, which contributes to the higher infiltration capacity of mixed slope compared to the other three types of slope [57].

In this study, the seepage analysis revealed that mixed planting and herbaceous planting significantly increase the slope's water infiltration capacity, contrary to the conclusions drawn in references [14,54], but consistent with references [52,55]. Therefore, although vegetation is often reported to affect soil permeability and water retention [28], the findings of this study indicate that this influence is not absolute but is determined by more complex factors. Specifically, this discrepancy can be attributed to the varying effects of vegetation on slope seepage regulation, influenced by factors such as vegetation species, growth cycles, slope soil types, compaction, as well as rainfall characteristics, intensity, and boundary conditions [58,59].

6.2. Effects of Vegetation on Slope Stability

The decrease in slope stability during rainfall is primarily caused by the increase in moisture content, which leads to a decrease in matric suction and subsequently reduces shear strength [60,61]. Natural rainfall experiments have shown that both herbaceous and mixed vegetation enhance the infiltration of rainfall into the slope. However, the

stability of mixed and herbaceous slopes is higher compared to bare soil slope, which seems contradictory. In fact, rainfall infiltration significantly affects soil moisture in the rhizosphere but has little impact on soil moisture in the deeper layers of the slope. And when analyzing slope infiltration, we found that the peak infiltration rate is only significant at a depth of 0.2 m, but becomes very small at greater depths. Therefore, vegetation increasing rainfall infiltration on slope does not affect the stability of the deeper layers of the slope [56]. Furthermore, at higher moisture content levels, there is a greater increase in cohesion of root-soil composite. Despite the larger rainfall infiltration in mixed and herbaceous slope, their increase in shear strength compared to bare soil slope is even greater. Therefore, the increase in internal moisture content of mixed and herbaceous vegetation slope does not surpass the stabilizing capacity of vegetation. In other words, the positive effect of vegetation roots in reinforcing and anchoring the slope outweighs the negative effect of rainfall infiltration on the slope [62,63].

6.3. Limitation

While this study provides valuable insights into the effects of vegetation on slope stability under rainfall conditions, it is important to acknowledge the limitations and simplifying assumptions inherent in our methodological approach, which should be considered when interpreting the results.

The numerical stability analysis was conducted in a two-dimensional plane, simplifying the root system of magnolia multiflora into anchor rods is a simplified approach. The assumption of uniformity in the out-of-plane direction may exaggerate the mechanical reinforcement effect of simulated anchor rods (representing shrub roots), particularly their continuity and tensile resistance. Consequently, the stability enhancements attributed to shrub and mixed vegetation, as quantified by the factor of safety, should be viewed as relatively conservative estimates. A more realistic three-dimensional analysis might yield a less pronounced but potentially more accurate assessment of root reinforcement.

The soil properties across all slope models were assumed to be homogeneous. Although great care was taken during model construction to ensure consistency, this simplification does not fully capture the natural spatial variability of soil characteristics (composition, density, hydraulic properties) encountered in field conditions, which could influence both infiltration patterns and mechanical behavior.

The initial volumetric water content differed between the slopes prior to rainfall, notably for the shrub-covered slope (27.96%) and the mixed vegetation slope (29.16%). This variation, though relatively small, likely contributed to the observed differences in pre-rainfall safety factors. The lower initial moisture content in the shrub slope would have resulted in higher initial matric suction and shear strength parameters, thereby enhancing its apparent stability compared to the mixed slope. Therefore, while vegetation type plays a significant role, attributing the pre-rainfall stability difference solely to the root architecture overlooks the confounding effect of initial hydrological conditions.

The findings are based on two specific plant species (cynodon dactylon and magnolia multiflora). The generalization of these results to other species with different root architectures (taproot and fibrous), drought resistances, and growth rates should be made with caution. Different species combinations might yield contrasting outcomes. This experiment captured the short-term effects during a single rainfall event. Long-term processes, such as root decomposition, ecological succession, and interspecies competition, which could significantly alter the soil structure and reinforcement mechanisms over time, were not investigated. The rainfall scenario (40.5 mm over 9 h) represents only one hydrological condition. The performance of vegetation, especially mixed planting, might differ under more extreme conditions (intense short-duration storms or prolonged drought followed by rain),

which are expected to become more frequent under climate change. Future research should incorporate long-term monitoring and a wider range of climatic scenarios to validate and extend the present findings.

7. Conclusions

This study is based on outdoor large-scale slope model experiments under a specific rainfall condition and for selected vegetation species. The experimental slope includes bare, herbaceous, shrub, and mixed herb–shrub slope. Combining unsaturated soil direct shear tests and numerical simulations, numerical models of four slopes are established, considering the weakening effect of water on shear strength parameters and the influence of root systems. The aim is to explore the influence mechanism of different vegetation types on slope rainfall infiltration and stability under rainfall, and provide scientific basis for the selection and optimization of ecological slope protection vegetation. The following major findings were obtained:

1. Under rainfall conditions, the infiltration rate of the slope exhibits significant spatial variability. The peak rainfall infiltration rates for all four types of slopes occur at a burial depth of 0.2 m, gradually decreasing with increasing burial depth. Various types of vegetation have distinct impacts on the regulation of a slope's infiltration capacity. The presence of herbaceous and mixed vegetation encourages rainfall infiltrate, resulting in a significant increase in cumulative infiltration by 21.32% and 77.07%, compared to the bare slope. In contrast, the infiltration rate and cumulative infiltration of shrub slope are lower than that of bare slope, leading to a decrease in cumulative infiltration by 61.06%.
2. When the moisture content was the same, the mixed roots soil had the highest shear strength, followed by shrub, herbaceous and bare soil. As the moisture content increased, the shear strength gradually decreased. Under elevated water content conditions, root systems exhibit a substantially stronger enhancement effect on soil cohesion compared to the improvement in internal friction angle.
3. The enhancement effect of vegetation on slope stability varies significantly depending on vegetation type. Before rainfall, the shrub slope exhibited the highest safety factor, reaching 3.046, followed by the mixed slope (2.948) and the herbaceous slope (2.81). The safety factors for the shrub, mixed and herbaceous slopes increased by 0.280, 0.182 and 0.044, compared to the bare slope's safety factor of 2.766. This difference is primarily due to the lower initial moisture content of the shrub slope, resulting in a more substantial increase in shear strength parameters and ultimately leading to a higher safety factor than the mixed slope.
4. As rainfall continues, the moisture content within each slope gradually tends towards saturation, reducing the differences between them. After rainfall, the mixed slope exhibits the highest safety factor at 1.361, followed by the shrub slope (1.275) and the herbaceous slope (1.192), The safety factors for the mixed, shrub and herbaceous slopes increased by 0.222, 0.136 and 0.053, compared to the bare slope's safety factor of 1.139. Therefore, under the experimental conditions, the mixed herb–shrub vegetation scheme showed a potential synergistic effect.

Author Contributions: Conceptualization, G.T. and L.G.; formal analysis, H.X., Q.C. and S.N.; data curation, L.G.; writing—original draft preparation, L.G.; writing—review and editing, L.G.; supervision, G.T., S.F. and Z.W. The results were discussed and conclusions were drafted jointly by all authors. All authors have read and agreed to the published version of the manuscript.

Funding: The authors would like to acknowledge financial support from the Joint Funds of the National Nature Science Foundation of China (No. U22A20232), Innovation Research Group Project

of the Hubei Provincial Department of Science and Technology (2025AFA020), Supported by Open Project Funding of Key Laboratory of Intelligent Health Perception and Ecological Restoration of Rivers and Lakes, Ministry of Education (HGKFZ07), Innovation Research Team Project of the Hubei Provincial Department of Science and Technology (JCZRQT202500027) and the International Collaborative Research Fund for Young Scholars in the Innovation Demonstration Base of Ecological Environment Geotechnical and Ecological Restoration of Rivers and Lakes.

Institutional Review Board Statement: Not applicable.

Informed Consent Statement: Not applicable.

Data Availability Statement: The original contributions presented in this study are included in the article. Further inquiries can be directed to the corresponding author.

Acknowledgments: We extend our sincere gratitude to Zhang Zhiyong for his assistance in data curation, and to Yang Hong for his support in the writing—original draft preparation.

Conflicts of Interest: The authors declare no conflict of interest.

References

1. Glade, T.; Anderson, M.G.; Crozier, M.J. *Landslide Hazard and Risk*; Wiley Online Library: Hoboken, NJ, USA, 2005.
2. Schuster, R.L.; Highland, L.M. The Third Hans Cloos Lecture. Urban landslides: Socioeconomic impacts and overview of mitigative strategies. *Bull. Eng. Geol. Environ.* **2007**, *66*, 1–27. [CrossRef]
3. Salciarini, D.; Fanelli, G.; Tamagnini, C. A probabilistic model for rainfall-induced shallow landslide prediction at the regional scale. *Landslides* **2017**, *14*, 1731–1746. [CrossRef]
4. Zhang, J.; Qiu, H.; Tang, B.; Yang, D.; Liu, Y.; Liu, Z.; Ye, B.; Zhou, W.; Zhu, Y. Accelerating effect of vegetation on the instability of rainfall-induced shallow landslides. *Remote Sens.* **2022**, *14*, 5743. [CrossRef]
5. Chirico, B.G.; Borga, M.; Tarolli, P.; Rigon, R.; Preti, F. Role of vegetation on slope stability under transient unsaturated conditions. *Procedia Environ. Sci.* **2013**, *19*, 932–941. [CrossRef]
6. Ruangpan, L.; Vojinovic, Z.; Di Sabatino, S.; Leo, L.S.; Capobianco, V.; Oen, A.M.P.; McClain, M.E.; Lopez-Gunn, E. Nature-based solutions for hydro-meteorological risk reduction: A state-of-the-art review of the research area. *Nat. Hazards Earth Syst. Sci.* **2020**, *20*, 243–270. [CrossRef]
7. Tongsan, L.; Bao, H.; Lan, H.X.; Zheng, H.; Yan, C.G.; Peng, J.B. Hydro-mechanical effects of vegetation on slope stability: A review. *Sci. Total Environ.* **2024**, *171691*, 0048–9697. [CrossRef]
8. Federico, P.; Vittoria, C.; Paola, S. Soil and Water Bioengineering (SWB) is and has always been a nature-based solution (NBS): A reasoned comparison of terms and definitions. *Ecol. Eng.* **2022**, *181*, 106687. [CrossRef]
9. Cerdà, A. The influence of geomorphological position and vegetation cover on the erosional and hydrological processes on a Mediterranean hillslope. *Hydrol. Process.* **1998**, *12*, 661–671. [CrossRef]
10. Michael, T.L.; Clemens, G.; Camilla, W.; Stefan, Z. The influence of herbaerous vegetation on slopo stability—A review. *Earth-Sci. Rev.* **2020**, *209*, 103328. [CrossRef]
11. Marzini, L.; Papasidero, M.P.; D'Addario, E.; Schwarz, M.; Disperati, L. Exploring the relationship between saturated hydraulic conductivity and roots distribution: Two case studies in Garfagnana (Northem Tuscany, Italy) and Zollikofen (Bern, Switzerland). *Front. Sustain.* **2025**, *6*, 1631482. [CrossRef]
12. Marzini, L.; D'Addario, E.; Papasidero, M.P.; Chianucci, F.; Disperati, L. Influence of root reinforcement on shallow landslide distribution: A case study in Garfagnana (Northem Tuscany, Italy). *Geosciences* **2023**, *13*, 326. [CrossRef]
13. Wu, H.W.; Chen, S.Y.; Pang, Y.W. Parametric study of effects of rain infiltration unsaturated slope. *Rock Soil Mech.* **1999**, *20*, 1–14. [CrossRef]
14. Nguyen, D.T.; Dau, N.V.; Ta, D.Q. The effects of rainfall on the stability of soil slopes in Khanh Vinh district, Khanh Hoa province. *Sci. Technol. Dev. J.* **2016**, *19*, 45–58. [CrossRef]
15. Qi, G.Q.; Hu, L.W. Study on mechanism and application of slope protection with vegetation. *Chin. J. Rock Mech. Eng.* **2006**, *25*, 2220–2225. [CrossRef]
16. Ng, C.W.W.; Ni, J.J.; Leung, K.A.; Zhou, C.; Wang, Z.J. Effects of planting density on tree growth and induced soil suction. *Géotechnique* **2016**, *66*, 711–724. [CrossRef]
17. Mao, Z.J.; Zhang, J.G.; Bi, Y.L.; Sun, W.B.; An, N. Numerical analysis of the time effect of purple clover on shallow damage protection of loess slopes. *Trans. Chin. Soc. Agric. Eng.* **2022**, *38*, 72–83. [CrossRef]
18. Yang, W.Z.; Han, S.F. Soil water ecological environment on the man-made woodland and grassland in loess hilly region. *Mem. Niswc Acad. Sin.* **1985**, *2*, 18–28.

19. Leung, T.F.; Yan, W.M.; Hau, C.B.; Tham, L.G. Root systems of native shrubs and trees in Hong Kong and their effects on enhancing slope stability. *Catena* **2015**, *125*, 102–110. [CrossRef]
20. Yu, Q.; Qiao, N.; Lu, H.; Hu, X.; Li, G.; Zhu, H. Effect study of plant roots reinforcement on soil. *Chin. J. Rock Mech. Eng.* **2012**, *31*, 3216–3223.
21. Yildiz, A.; Graf, F.; Springman, S.M. An investigation of plant-induced suction and its implications for slope stability. *Proc. Inst. Civ. Eng.-Geotech. Eng.* **2019**, *172*, 520–529. [CrossRef]
22. Yi, H.J.; Zhang, X.P.; He, L.; Zou, Y.D.; Lv, D.; Xu, X.M.; He, J.; Wang, Y.C.; Tian, Q.L. Vegetation restoration potential and land use change in different geomorphological areas of the Loess Plateau. *Trans. Chin. Soc. Agric. Eng.* **2022**, *38*, 255–263. [CrossRef]
23. Cheng, P.; Li, J.H.; Song, L. Hydraulic and mechanical characteristics of ecological slopes: Experimental study. *Chin. J. Geotech. Eng.* **2017**, *39*, 1901–1907. [CrossRef]
24. Ji, X.L.; Yang, P. The exploration of the slope displacement with vegetation protection under different rainfall intensity. *J. For. Eng.* **2020**, *5*, 127–133. [CrossRef]
25. Kokutse, N.K.; Temgoua, A.G.T.; Kavazović, Z. Slope stability and vegetation: Conceptual and numerical investigation of mechanical effects. *Ecol. Eng.* **2016**, *86*, 146–153. [CrossRef]
26. Xiao, T.; Li, P.; Hou, Y.F.; Liu, Y.M. A review of research on vegetated slope protection. *J. Eng. Geol.* **2019**, *27*, 379–385. [CrossRef]
27. Tiwai, R.; Bhandary, N.; Yatabe, R.; Bhat, D. New numerical scheme in the finite-element method for evaluating the root-reinforcement effect on soil slope stability. *Geotechnique* **2013**, *63*, 129–139. [CrossRef]
28. Jotisankasa, A.; Sirirattanachat, T. Effects of grass roots on soil-water retention curve and permeability function. *Can. Geotech. J.* **2017**, *54*, 1612–1622. [CrossRef]
29. Zhang, L.W.; Chen, Y.Y.; Wang, K.; Liang, Z.C.; Liang, Y.T. Cooling effect of urban wetlands under its influencing factors under different meteorological conditions in Wuhan, China. *Resour. Environ. Yangtze Basin* **2022**, *31*, 1938–1952. [CrossRef]
30. *GB/T 50123-2019*; Standard for Geotechnical Testing Method. China Planning Press: Beijing, China, 2019.
31. Xu, T.; Liu, C.Y.; Hu, X.C.; Xu, Z.W.; Shen, Z.Y.; Yu, D.M. Mechanical effects of vegetation protection on slope under loading conditions in loess areas of Xining Basin. *Trans. Chin. Soc. Agric. Eng* **2021**, *37*, 142–151. [CrossRef]
32. Li, A.G.; Yue, Z.Q.; Tham, L.G.; Lee, C.F.; Law, K.T. Field-monitored variations of soil moisture and matric suction in a saprolite slope. *Can. Geotech. J.* **2005**, *42*, 13–26. [CrossRef]
33. Li, Z.; Wu, P.T.; Feng, H.; Zhao, X.N.; Huang, J.; Zhuang, W.H. Simulated experiment on effect of soil bulk density on soil infiltration capacity. *Trans. Chin. Soc. Agric. Eng.* **2009**, *25*, 40–45. [CrossRef]
34. Qin, F. Experimental Study on Influencing Factors of Soil Infiltration Rate and Cumulative Infiltration Amount on the Backslope of Reservoir. Master's Thesis, Shandong Agricultural University, Taian, China, 2020.
35. Van Genuchten, M.T. A closed-form equation for predicting the hydraulic conductivity of unsaturated soils. *Soil Sci. Soc. Am. J.* **1980**, *44*, 892–898. [CrossRef]
36. Wang, L.R.; Yan, Y.; Shang, C.J.; Tan, J.; Yang, Y.Y. The soil stabilization and slope protection effects of two herbaceous plants on red clay slopes. *Bull. Soil Water Conserv.* **2024**, *44*, 146–154. [CrossRef]
37. Zhao, Y.J.; Hu, X.C.; Liu, C.Y.; Dou, Z.N.; Li, G.R. Experimental study on enhancing the shear strength of slope soil by plant roots in cold and dry environments. *Res. Soil Water Conserv.* **2016**, *23*, 212–220. [CrossRef]
38. Wang, X.; Li, Z.Y.; Xiao, H.B.; Liu, S.S.; Liu, J. Study on shear strength of plant slope based on soil-water characteristic curve. *J. Soil Water Conserv.* **2021**, *35*, 57–62, 71. [CrossRef]
39. Kalenchuk, K.S.; Hutchinson, D.J.; Diederichs, M.S. Downie Slide: Numerical simulation of groundwater fluctuations influencing the behaviour of a massive landslide. *Bull. Eng. Geol. Environ.* **2013**, *72*, 397–412. [CrossRef]
40. Zhan, L.T.; Li, H.; Chen, Y.M.; Fredlund, D.G. Parametric analyses of intensity-duration curve for predicting rainfall-induced landslides in residual soil slope in Southeastern coastal areas of China. *Rock Soil Mech* **2012**, *33*, 872–880. [CrossRef]
41. Richards, L.A. Capillary conduction of liquids through porous mediums. *Physics* **1931**, *1*, 318–333. [CrossRef]
42. Chen, Q.; Yang, X.G.; Zhou, J.W. Assessing the mechanical effects of vegetation on the stability of slopes with different geometries and soil types. *Bull. Eng. Geol. Environ.* **2024**, *83*, 8. [CrossRef]
43. Zhang, L.Y.; Zheng, Y.R.; Zhao, S.Y.; Shi, W.M. The feasibility study of strength-reduction method with FEM for calculating safety factors of soil slope stability. *J. Hydraul. Eng.* **2003**, *1*, 21–26. [CrossRef]
44. Liu, A.L. Study on Strengthening Effect of Mulan. Master's Thesis, Central South University of Forestry and Technology, Changsha, China, 2022.
45. Tan, L. The Experimental Study on the Mechanical Properties of Soil Reinforcement. Master's Thesis, Central South University of Forestry and Technology, Changsha, China, 2017; pp. 50–52.
46. Li, T.; Wang, Y.Q.; He, Y.C.; Qi, Z.H.; Luo, P.Z. Influences of three typical trees on slope deformation and stability under wind load. *Trans. Chin. Soc. Agric. Eng.* **2023**, *39*, 110–119. [CrossRef]
47. Jia, C.Q.; Huang, M.S.; Wang, G.H. Stability analysis of soil slopes under unsaturated unsteady seepage using strength reduction finite element method. *J. Rock Mech. Geotech. Eng.* **2007**, *26*, 1290–1296.

48. Wang, C.L.; Tang, D.; Li, Y.F.; Jiang, Z.M.; Wang, Y.X. Slope stability analysis based on considering the influence of moisture content on soil shear strength parameters. *Technol. Innov. Appl.* **2024**, *14*, 61–64. [CrossRef]
49. Coppin, N.J.; Richards, I.G. *Use of Vegetation in Civil Engineering*; Construction Industry Research and Information Association: London, UK, 1990.
50. Likitlersuang, S.; Takahashi, A.; Eab, K.H. Modeling of root-reinforced soil slope under rainfall condition. *Eng. J.* **2017**, *21*, 123–132. [CrossRef]
51. Xu, H.; Yuan, H.L.; Wang, X.Y.; Wang, D.; Chen, J.X.; Rong, C.Q. Influences of morphology and hierarchy of roots on mechanical characteristics of root-soil composites. *Chin. J. Geotech. Eng.* **2022**, *44*, 926–935. [CrossRef]
52. Huang, S.P.; Chen, J.Y.; Xiao, H.L.; Tao, G.L. Test on rules of rainfall infiltration and runoff erosion on vegetated slopes with different gradients. *Rock Soil Mech.* **2022**, *44*, 3435–3447. [CrossRef]
53. Kong, G.Q.; Wen, L.; Liu, H.L.; Wang, C.Q. Strength properties of root compound soil and morphological observation of plant root. *Rock Soil Mech.* **2019**, *40*, 3717–3723. [CrossRef]
54. Buczko, U.; Bens, O.; Hüttl, R.F. Changes in soil water repellency in a pine–beech forest transformation chronosequence: Influence of antecedent rainfall and air temperatures. *Ecol. Eng.* **2007**, *31*, 154–164. [CrossRef]
55. Li, J.X.; He, B.H.; Chen, Y. Root features of typical herb plants for hillslope protection and their effects on soil infiltration. *Acta Ecol. Sin.* **2013**, *33*, 1535–1544. [CrossRef]
56. Peng, S.S. Research on the Effect of the Biotechnical Slopeprotection on the Shallow Stability. Ph.D. Thesis, Chinese Academy of Sciences, Beijing, China, 2007.
57. Wan, J.; Xiao, H.L.; He, J.; Li, L.H. Analysis of influence factors on the growth of grass-shrub vegetation in highway slope. *Highway* **2014**, *59*, 200–204.
58. Wu, H.W. Atmosphere-plant-soil interactions: Theories and mechanisms. *Chin. J. Geotech. Eng.* **2017**, *39*, 1–47. [CrossRef]
59. Das, S.; Narula, P.; Sarkar, K. Design of intermittent rainfall-pattern for structures with gridded data: Validation and implementation. *J. Build. Eng.* **2020**, *27*, 100939. [CrossRef]
60. Calvello, M.; Cascini, L.; Sorbino, G. A numerical procedure for predicting rainfall-induced movements of active landslides along pre-existing slip surfaces. *Int. J. Numer. Anal. Methods Geomech.* **2008**, *32*, 327–351. [CrossRef]
61. Das, P. Reconstruction of a wetting-induced shallow landslide in Shillong, India. *Proc. Inst. Civ. Eng.-Forensic Eng.* **2020**, *173*, 48–53. [CrossRef]
62. Sun, H.; Wu, G.; Song, J.Y.; Wang, Y. Technology parameters of stability in subgrade slope of vegetation. *Clin. J. Gastroenterol.* **2010**, *32*, 594–597.
63. Feng, S.; Liu, H.W.; Ng, C.W.W. Analytical analysis of the mechanical and hydrological effects of vegetation on shallow slope stability. *Comput. Geotech.* **2019**, *118*, 103335. [CrossRef]